APPLICATION OF PHOTO-CATALYST SILVER FERRITE OXIDE ON CANCER CELL TREATMENT

CHUAH XUI FANG

A project report submitted in partial fulfilment of the requirements for the award of Bachelor of Engineering (Hons.) Chemical Engineering

Faculty of Engineering and Science
Universiti Tunku Abdul Rahman

May 2016

DECLARATION

I hereby declare that this project report is based on my original work except for citations and quotations which have been duly acknowledged. I also declare that it has not been previously and concurrently submitted for any other degree or award at UTAR or other institutions.

Signature : _____

Name : Chuah Xui Fang

ID No. : 11UEB03170

Date : 12.5.2016

APPROVAL FOR SUBMISSION

I certify that this project report entitled **"APPLICATION OF PHOTO-CATALYST SILVER FERRITE OXIDE ON CANCER CELL TREATMENT"** was prepared by **CHUAH XUI FANG** has met the required standard for submission in partial fulfilment of the requirements for the award of Bachelor of Engineering (Hons.) Chemical Engineering at Universiti Tunku Abdul Rahman.

Approved by,

Signature : _____

Supervisor : Dr. Lee Poh Foong

Date : 12.5.2016

Specially dedicated to
my beloved grandparents, mother and father.

ACKNOWLEDGEMENTS

I would like to thank everyone who had contributed to the successful completion of this project. I would like to express my gratitude to my research supervisor, Dr. Lee Poh Foong and co-supervisor, Ir. Teoh Hui Chieh for their invaluable advice, guidance and their enormous patience throughout the development of the research.

I would like express my deepest appreciation to Prof. Lu Shih-Yuan and Dr. Lee Kuan-Ting from National Tsing Hua University, Taiwan for their precious opinion and invaluable advice throughout the research.

In addition, I would like to thank my seniors, Mr. Teoh Boon Yew and Mr. Lee Jia Ji and lab assistant, Miss Heng Sze Lu for their valuable helps on my research.

Besides, I would like to express my gratitude to my loving parent, sisters and friends who had helped and given me encouragement in completing this research. Lastly, I would like to sincerely thank everyone who had relentless helping me out and guiding me throughout the research until completion.

APPLICATION OF PHOTO-CATALYST SILVER FERRITE OXIDE ON CANCER CELL TREATMENT

ABSTRACT

The application of photo-catalyst $Ag_2Fe_2O_4$ in cancer cell treatment, particularly on HeLa cell (cervical cancer cell) was investigated. Photo-catalyst can be excited upon exposure to light to generate Reactive Oxygen Species (ROS) which is responsible for the cancer cell treatment. An UV-transilluminator (Gel Imaging 112) which emitted wavelength of 365 nm was used in the treatment. The characterization of photo-catalyst $Ag_2Fe_2O_4$ was done by using X-Ray Diffraction (XRD), High Resolution Transmission Energy Microscopy (HRTEM), Energy Dispersive X-ray Spectroscopy (EDX) and UV-Visible Spectrophotometer. The particle grain size and bandgap energy of photo-catalyst $Ag_2Fe_2O_4$ was 6.7 nm and 2.0 eV with cut-off wavelength of 620 nm respectively. Two parameters (concentration of photo-catalyst and total irradiation time) were studied in this project. Different concentration of photo-catalyst $Ag_2Fe_2O_4$ varied from 20 µg/mL, 40 µg/mL and 60 µg/mL and different total irradiation time from 5 minutes to 30 minutes with interval of 5 minutes were tested to study the effect of photo-catalyst concentration and exposure of UV light towards cancer cell treatment. Cell viability and morphology of cells before treatment, after treatment and regrowth after 24 hours of treatment were determined to investigate the result of cancer cell treatment. It was found $Ag_2Fe_2O_4$ can remarkably induce apoptosis in HeLa cell (23.89 % of cell viability after treatment) with exposure of 30 minutes to UV light irradiation coupled with 40 µg/mL of photo-catalyst $Ag_2Fe_2O_4$, which has the best performance amongst.

TABLE OF CONTENTS

LIST OF TABLES

LIST OF FIGURES

LIST OF SYMBOLS / ABBREVIATIONS

e^-	excited electron
h	Plank's constant
h^+	holes pairs
L	crystallite size at (h k l) plan
λ	X-ray wavelength of radiation for CuKα
M	concentration, µg/mL
$NO\bullet$	nitric oxide
O_2^-	superoxide anion
$OH\bullet$	hydroxyl radicals
$ROO\bullet$	peroxyl radicals
v	velocity of light
V	volume, mL

EDX	energy dispersive X-ray spectroscopy
FBS	fetal bovine serum
FWHM	full width at half maximum
HRTEM	high resolution transmission electron microscope
JCPDS	Joint Committee on Powder Diffraction Standard
PBS	phosphate buffered saline
ROS	reactive oxygen species
RPMI	Roswell Park Memorial Institute
TEM	transmission electron microscope
UV-Vis	UV-visible
XRD	X-Ray Diffraction

LIST OF APPENDICES

CHAPTER 1

INTRODUCTION

1.1 Background

According to the study done by National Cancer Institute based on the postulation from the data from year 2010 to 2012, it is estimated that there will be 1 658 370 new cases of cancer diagnosis in the United States and 589 430 cancer related death. Cancer is predicted to be the leading cause of death in the United States. Furthermore, in Malaysia, there is an increment of 14.4 % in cancer cases from year 2008 to 2012. The number of new cancer cases is expected to increase to 56 932 from 37 400 by 2025 if appropriate action is not taken (Jemal et al., 2004).

1.2 Cancer Treatment

Current medical treatments for cancer includes surgery, radiotherapy, chemotherapy, hormone therapy as well as stem cell transplant. Unfortunately, these treatment options often bring side effects to the patients, some side effects can even take over their daily life. Therefore, developing a new technology or treatment option that able to minimize the side effect of cancer treatment is one of the objective of oncologists and scientists.

Application of photo-catalyst to cancer treatment is a new approach to the development of cancer treatment technology. A photo-catalyst is defined as a

substance that alter the rate of reaction of a catalyzed reaction by absorbing the light (Serpone and Emeline, 2002). Photosynthesis is a typical example of photo-catalysis reaction while chlorophyll serves as the photo-catalyst of this system. Photo-catalyst is widely applied in waste water treatment, air purifying, anti-microbial as well as killing tumor cell (Zhang and Sun, 2004).

Over the few years, application of photo-catalyst in cancer treatment grabs the attention from scientists and it is believed to be a promising alternative to the typical treatment option that leads to severe side effect. Currently, according to the finding of Huang et al. (2012) on the photocatalytic performance of TiO_2 doped with CdS quantum dots in cancer cell treatment, the cancer cell killing efficiency of the photo-catalyst is found to reach 80.5 % under light treatment.

1.3 How Photo-catalyst Kills Cancer Cell

The common catalysts that are being applied in photocatalytic cancer cell treatment are titanium oxide (Zhang et al., 2014) and zinc oxide (Kleinsasser, 2010). The mechanism that involved in the killing of cancer cell by using photo-catalyst is believed to be related to the reactive oxygen species that is being produced as the product of photo-catalysis reaction.

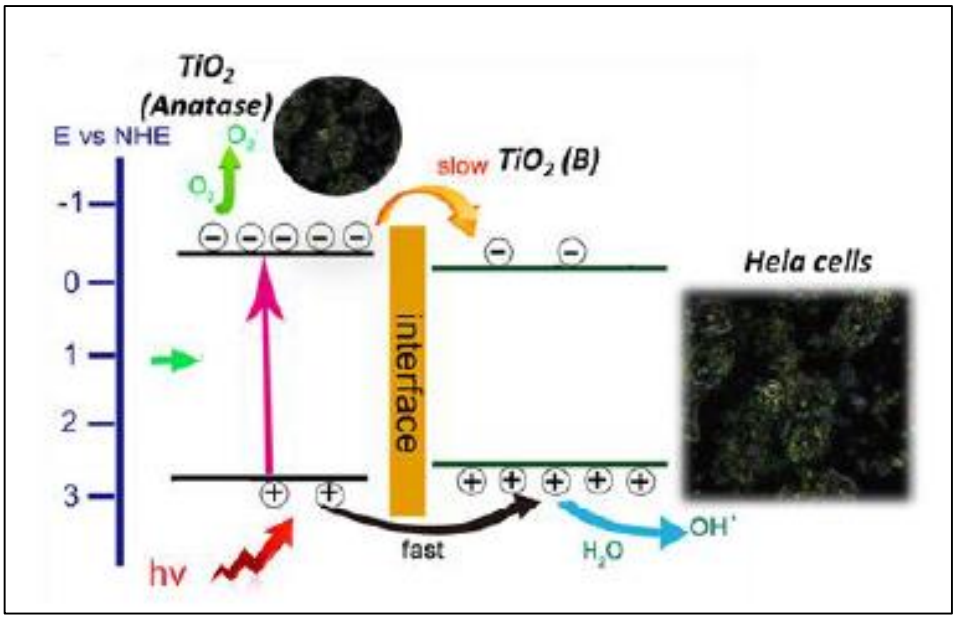

Figure 1.1: Illustration of the Mechanism of Photo-Catalyst on Cancer Cell Treatment. (Zhang et al., 2014)

Reactive oxygen species are the reactive molecules or free radicals that derived from oxygen molecule. Reactive oxygen species can be naturally found in human body as the by-products of aerobic metabolism (mitochondrial electron transport during aerobic respiration) or by oxidoreductase enzymes (Held, 2015). Reactive oxygen species that produced from mitochondria is known as mitochondrial reactive oxygen species (Sullivan and Chandel, 2014). On the other hand, reactive oxygen species is also generated during the metal catalyzed oxidation. The reactive oxygen species is believed to be able to kill the cancer cell by disrupt or damage the membrane and interior of the tumor cell which lead to the death of cancer cells based on apoptosis as well as neurosis (Townley, Kim and Dobson, 2012).

1.3.1 Silver Ferrite Oxide

Silver oxide ferrite with the chemical formula of $Ag_2Fe_2O_4$ is a spinel-structured catalyst. Typical spinel catalyst has a chemical formula of AB_2X_4 where A is a divalent ion, B is a trivalent ion and X is an oxide ion (Deer, Howie and Zussman,

1992). Most commonly used spinel-structured of catalyst consists of Fe_2O_3, $ZnFe_2O_4$, $NiFe_2O_4$ and $CoFe_2O_4$ (Kong et al., 2011). In $Ag_2Fe_2O_4$, two Ag ions are needed to reach the stable state of molecule as Ag ion is a monovalent cation.

Previous studies found that catalyst with spinel structure has excellent performance in catalysis, hence, it is widely applied in photo-degradation of organic pollutant (Jiang et al., 2011), photocatalytic hydrogen production (Yu et al., 2013) and biosensor (Wayu et al., 2015). Since spinel catalyst has excellent catalytic performance in various fields as reported, it is expected that $AgFe_2O_4$ has satisfactory performance in the photocatalytic of cancer cell treatment.

Besides, $Ag_2Fe_2O_4$ is an oxide semiconductor which will generate electrons and holes pairs upon photo-irradiation. Photo-generated electrons and holes pairs are found useful in the formation of free radicals that are toxic to cancer cells (Cai et al., 1992).

1.4 Problem Statement

Typical cancer treatment options bring a lot of side effects to the patients, some patients even suffering from the side effects and critically affect their daily life. This is because typical cancer treatment options inactivate cancer cell but at the same time bring harmful effect to the normal healthy cell.

Many approaches had been performed to enhance the cancer treatment to minimize the side effect. Photocatalytic in cancer cell killing might be a promising option to treat cancer patient which offers the minimum side effect.

Silver ferrite oxide, $Ag_2Fe_2O_4$ photo-catalyst is chosen as the catalyst of this research due to the element of silver in this catalyst. Silver particles are widely used in medical application due to its superior performance in preventing microbial infections (Alexander, 2009). Silver particle is also found to have excellent performance in wound healing, diagnosis and pharmacological treatment (Xing et al.,

2014). However, silver particle has a drawback of being comparatively expensive, makes the treatment that involving silver particles economically unfeasible (Gomatam and Mittal, 2008). Therefore, $Ag_2Fe_2O_4$ is chosen as the object of this research, aims to determine the efficiency of $Ag_2Fe_2O_4$ in medical applications and evaluate the possibility of this catalyst as the alternative of pure silver.

1.5 Aims and Objectives

The aim of this research is to determine the feasibility of catalyst on the application of cancer treatment. The catalyst of interest of this research is silver ferrite oxide, $Ag_2Fe_2O_4$ while the cancer cells of interest is HeLa cell.

Generally, the main objective of this research is to investigate the effect of the application of the catalyst on cancer cell treatment. The parameters of this research include the concentration of the catalyst, the exposure time of the catalyst to the cancer cell as well as the presence of the light source during the treatment. In other words, the specific objectives are as outline below:

1. To investigate the effect of the presence of light source on the cancer cell treatment.
2. To investigate the effect of different concentration of catalyst on the cancer cell treatment.
3. To investigate the effect of different exposure time on the cancer cell treatment.

CHAPTER 2

LITERATURE REVIEW

2.1 Cancer

Cancer is one of the leading causes of mortality as well as morbidity worldwide. Generally, cancer is a term that used to describe a class of diseases that characterized to be out-of-control cell growth and behave differently from the cell type they originate. All organisms grow from a single cell and undergo mitosis process, in which a single cell (parent cell) splits into two identical sets of cell, so called daughter cells that duplicate the information from the parent cell. In a healthy system, the mitosis will continue to split and grow new cells in order to replace the dead cells as well as to repair the damaged cell (Crosta, 2008).

However, in cancer, either the dead cells are not replaced or the damaged cells are not replaced, instead, they start to grow and divide with an abnormal growth patterns, the information carried by the divided cells become altered. The abnormal cells continue to grow out of control and may grow into a tumor. There are two types of tumor, called benign and malignant, in which benign tumor is not life threatening with rare exceptions, while malignant tumor is cancerous. For each generation of new cells, the cells become a little less like the parent cells, hence, less effective at performing their designated tasks (Daniel, 2005). Diagram 2.1 shows a clear process on how a normal healthy cell grows and divide out of control and become a tumor.

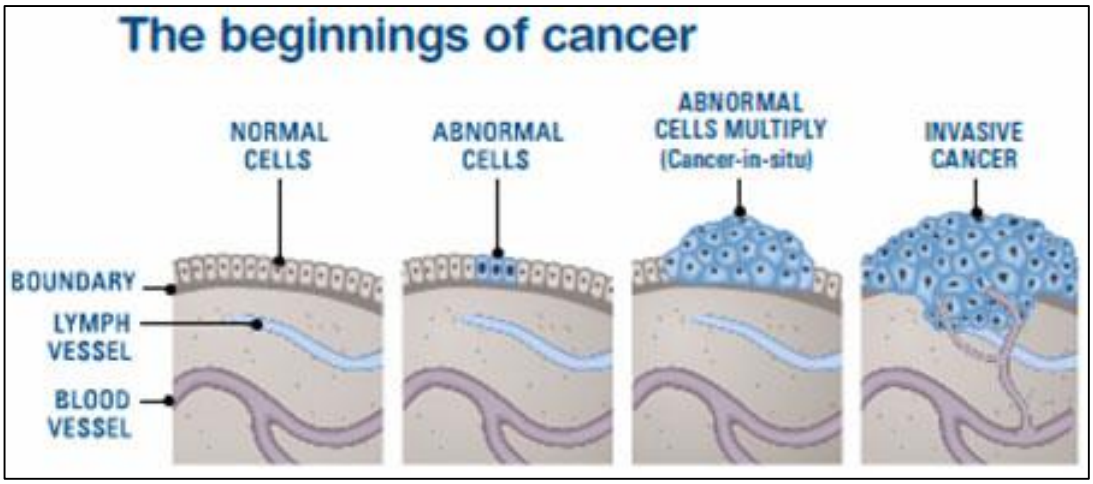

Figure 2.1: The Beginnings of Cancer. (Qureshi, 2014)

2.2 Cancer Treatment and Their Side Effects

There are various types of cancer treatment that suits various cancer types. Parameters that determine the applicability of treatments includes the type of cancer, the stage of the cancer, patient's age and health status. Generally, there will be combination of treatments, such as surgery with radiation therapy (Miller et al., 1981).

The principles of few current cancer treatment and their side effects will be discussed at this section. The cancer treatments that will be included at this section are as followed:

- Surgery
- Radiotherapy
- Chemotherapy

2.2.1 Surgery

If a cancer is not metastasized, it is most often recommended to employ surgery to remove the whole tumor, leaving behind as much of the normal tissues as possible. It is possible to completely cure a patient who has only primary cancer by surgery. Other than removing the tumor, surgery can also be used to diagnose cancer and determine the location of the cancer (Cancer.Net, 2011). When a tumor is removed, the oncologist will also take out some of the margin, which is the surrounding tissue to ensure that there is clear margin of healthy tissue around the entire tumor. If not, further surgery will usually be recommended or patient will be suggested to undergo chemotherapy or radiotherapy after the surgery.

Surgery is the known oldest cancer treatment, and it is possible to completely cure a cancer patient given that the patient is suffering from primary cancer. However, if the disease is already metastasized, it is nearly impossible to remove all the cancer cells from the body. In other words, removing cancer cells by surgery treatment method is only limited to primary cancer patient.

2.2.2 Radiotherapy

Radiotherapy utilizes the high energy rays, which is the gamma rays that emitted from either metal or X-ray to destroy or shrink the cancer cells. Radiotherapy is considered to be the most common type of cancer treatment. It can be the main treatment or the treatment after a surgery to target or eliminate any other potential remaining cancer cell (Daniel, 2005). High dose of radiation to the affected area can also lead to damages of the neighboring healthy cells and tissues. Fortunately, current technology allows it to be more precise in which the energy beam can be more accurately targeted, and enhance the performance of radiotherapy in terms of minimization of side effects.

According to Daniel (2005), it is possible for a survivor of radiotherapy to suffer from secondary cancer as a result of the radiotherapy treatment after some

time of the treatment. Furthermore, most of the patients claim that they experience fatigue after the treatment, compared to the fatigue that experienced by normal healthy individual, cancer-related fatigue is more distressing due to the poor immune system (Cancer.org, 2014). Exposure of radiation to the pelvic area (ovaries for women and testicles for men) might leads to infertility. Men receiving radiotherapy at the pelvic area will have reduced sperm activity as well as sperm production. For women, they might experience menopause and affect the fertility (Cancervic.org.au, 2014). Radiotherapy treatment brings less side effect as compared to chemotherapy.

2.2.3 Chemotherapy

Both surgery and radiotherapy are localized treatment, which means they deal with diseases that is localized in a particular area. When the disease is spread or metastasized, chemotherapy is used so that the treatment reach all parts of the body to eliminate cancer cells wherever they have lodged (Daniel, 2005). Instead of using high energy beam to destroy the cancer cell like radiotherapy, chemotherapy utilizes the anti-cancer drug to kill the cancer cells, exposing the entire body to cancer-fighting chemicals. Anti-cancer drugs work in several ways but they serve the same purpose, which is to stop the growth and division of cancer cell, preventing them from attacking the normal healthy cells. The aim of chemotherapy is to get rid of all the cancer cells and more importantly, is to recurrent cancer, which is the specific term used to describe the cancer that comes back after treatment.

Chemotherapy drugs are very powerful drugs that used to kill the fast growing cancer cell but it also destroys healthy cells. In terms of circulatory and immune systems, anti-cancer drugs reduce the amount of both red blood cells and white blood cells, as well as affect their effectiveness. Reduced number of white blood cells will result in neutropenia (abnormally low count of neutrophils). White blood cells are produced to fight against infection and low effectiveness of white blood cells will suppress or weaken the immune system.

On the other hand, exposing the entire body to the anti-cancer drug will lower the amount of red blood cells and lead to anemia, a specific term that used to describe a condition where the hemoglobin level in the blood stream is too little. Hemoglobin in a red blood cell is used to transport inhaled oxygen from the lungs to the entire body and transport the exhaled and unwanted carbon dioxide from the organs to the lungs. Anemia will makes the patient feel extremely fatigue (Healthline, 2015). Furthermore, according to de Boer-Dennert et al. (1997), in his survey towards 197 patients who undergo chemotherapy treatment, 80 % of all the patients experienced nausea and 57 % experienced vomiting, hair loss appeared to be more distressing in women.

2.3 HeLa Cell Line

HeLa cell lines are oldest and most commonly used in laboratory specifically for research purposes (Shen, 2013). It is originally obtained from cancerous cervical tissue. The cells exhibit epithelial morphology and it is an adherent type of cancer cells. Figure 2.2 shows the typical image of HeLa cell line where it is adherent to the surface of the T-flask.

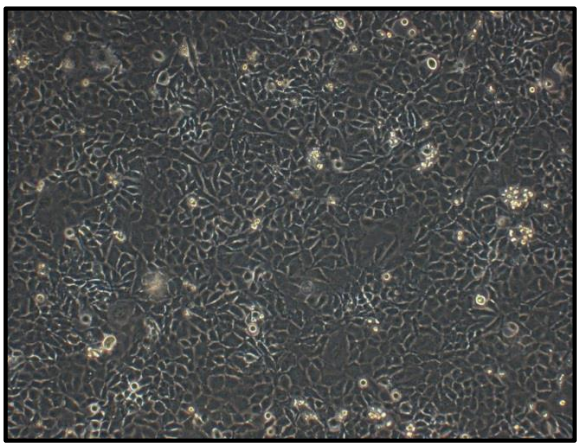

Figure 2.2: Typical Image of HeLa Cell Line (Cellresource.cn, 2009).

2.4 Photo-catalyst and Photo-catalytic Process

Photo-catalysis is an area engaging the attention of many researches today. There are a number of new avenues opened up in recent years, including photo-degradation of wastewater that consists of organic pollutants, photo-destruction of tumor cells and application as the material of biosensor (Viswanathan, Sivasanker and Ramaswamy, 2002). Most commonly used photo-catalyst is titanium oxide, TiO_2 which had been commercialized in production and utilized in industrial processes especially in the treatment of wastewater that consists of organic pollutant (Chan et al., 2011).

According to the finding of Li (2013) on the photo-catalysis of oxide semiconductors, he believed that the interfacial redox reaction of electrons and holes pairs that are generated during bandgap excitement with light irradiation is responsive to the photo-catalytic effect. Band gap of the semiconductors plays an important role in the generation of electrons and holes pairs that will be further involved in the mechanism of production of free radicals that are responsive to the degradation of organic pollutants by destroying the structure of organic pollutants (Diwan and Murugan, 2013).

Band gap is defined as the difference in energy between valence band and conduction band, valence band is the electron orbitals that electrons are not free to move while conduction band is the orbitals that are relatively free and carry a current (Van Zeghbroeck, 2010). In other words, band gap energy is the minimum energy an electron received to be excited from valence band to conduction band for conduction purpose. Figure 2.3 illustrates the band gap energy of a semiconductor. The valance band is denoted as E_v, conduction band id denoted as E_c while band gap energy is denoted as E_g.

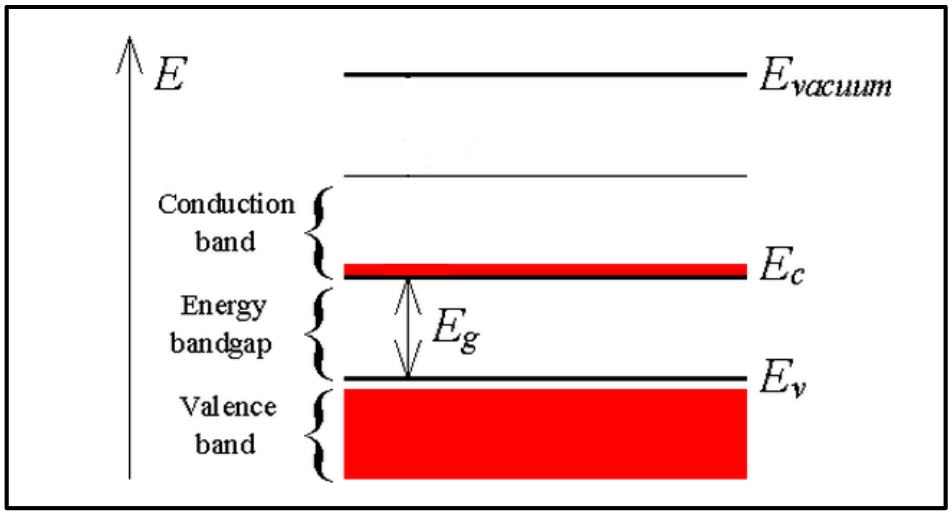

Figure 2.3: Energy Band Diagram of a Semiconductor. (Van Zeghbroeck, 2010)

The generation of electrons and holes pairs is believed to be dependent on the band gap energy. Small band gap energy favors the production of electrons and holes pair upon the light irradiation. When a photon carries the same amount or larger amount of energy with the band gap energy of the semiconductors in the form of *hv*, an electron is excited and transformed from the valence band to conduction band, leaving the valence band a hole. This phenomenon is known as photon adsorption and can be explained by reaction 2.1 as shown below, where e^- indicates the excited electron and h^+ denotes the holes pairs.

$$semiconductor \xrightarrow{hv} e^- + h^+ \quad (2.1)$$

The photo-generated electrons and holes pairs will further react with the surrounding water molecule and oxygen molecule to form powerful oxidative radicals, or reactive oxygen species which are reported to be toxic to cells (Cai et al., 1992). The mechanism of the formation of oxidative radicals are explained by the reaction below, from reaction 2.2 to reaction 2.6.

$$h^+ + H_2O \rightarrow \cdot OH + H^+ \quad (2.2)$$

$$e^- + O_2 \rightarrow O_2^- \quad (2.3)$$

$$O_2^- + H^+ \rightarrow HO_2 \cdot \quad (2.4)$$

$$2HO_2 \cdot \rightarrow O_2 + H_2O_2 \quad (2.5)$$

$$H_2O_2 + O_2^- \rightarrow \cdot OH + OH^- + O_2 \qquad (2.6)$$

The mechanism of the formation of free radicals in a photo-catalyst upon light excitement is illustrated in Figure 2.4 below. It is clearly shows in the figure that the electron from valence electron is being excited with the energy in the form of *hv*, migrated to conduction band, leaving a holes pairs in the valence band. The photo-excited electron reduces the surface oxygen to form superoxide anion (O_2^-). In other words, the oxygen molecule accepts the photo-generated electron. On the other hand, a water molecule is being oxidase by the holes pairs, forming a hydroxyl radicals (OH·). The formation of highly oxidizable OH· radicals and H_2O_2 are formed via reaction 2.4 and 2.5 respectively. Generally, experimental researchers shows that O_2^- is less reactive (Cai et al., 1992) and most of the degradation of organic compounds involved the OH· mechanism (Boonrattanakij, Lu and Anotai, 2009).

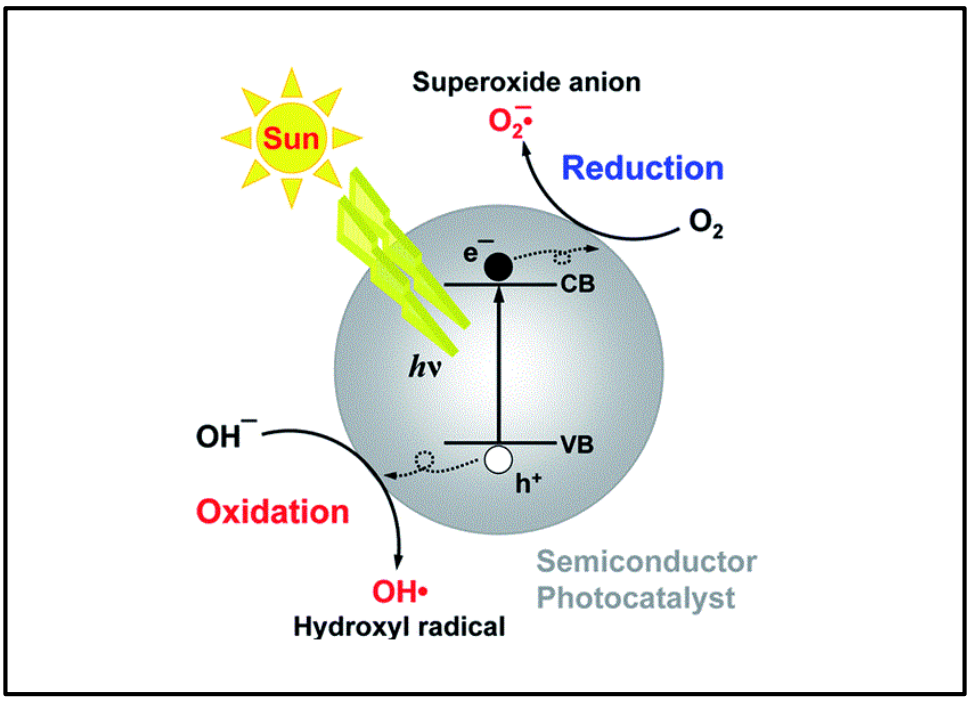

Figure 2.4: Photolysis Process of a Photo-Catalyst. (Djurišić, Leung and Ching Ng, 2014)

2.5 Roles of ROS in Cancer Cell Killing Mechanism

Reactive oxygen species (ROS) is a term that used to describe the species that consists one or more unpaired electron in their outermost electron shells. Due to the presence of unpaired electrons, ROS are generally highly reactive. The oxygen species can be either in radicals, ion or molecular form (Halliwell, 1991). Generally, ROS can be categorized into two groups, which are free-oxygen radicals and non-radical ROS. Free-oxygen radicals are superoxide anion (O_2^-), hydroxyl radical (OH·), nitric oxide (NO·), peroxyl radicals (ROO·) and etc. whereas non radical ROS are hydrogen peroxide (H_2O_2), singlet oxygen (O_2), highly reactive lipid or carbohydrate derived carbonyl compounds and etc. (Liou and Storz, 2010). Among them, superoxide anion, hydroxyl radical, hydrogen peroxide and singlet oxygen are oxygen-derived oxygen, which are highly toxic to cells as reported (Cai et al., 1992).

ROS can be found naturally in the cells and these ROS are termed intracellular ROS. Based on the previous studies, the major source of intracellular ROS is the NADPH oxidases, which is an enzyme that catalyze the production of superoxide anion and NADPH (Sullivan and Chandel, 2014). ROS are not always toxic to the cell, when the concentration of ROS in the cell is in a balance with antioxidants. ROS actually act as intracellular signaling messenger, involving in the regulation of cell proliferation, metabolic alterations and angiogenesis (Clerkin et al., 2008). Intracellular ROS generated are normally reduced by non-enzymatic and enzymatic anti-oxidants. Exposure of normal cells to the very high concentration of ROS, resulted from the imbalance of redox state as cellular antioxidants fail to reduce ROS, can damage cellular proteins, lipids and DNA. This gives rise to degenerative to cells, promotes DNA mutations and genetic instability, leading to the cancer formation (D'Autréaux and Toledano, 2007).

In spite of the fact that high level of ROS are oncogenic, ironically, ROS production is a mechanism shared by all non-surgical therapeutic approaches for cancers due to its ability in triggering cell death through apoptosis (Renschler, 2004). In other words, there is a ROS threshold level in tumor and non-tumor cell. Certain level of ROS is necessary for cell survival as ROS is responsive in signaling, however, overwhelming of ROS trigger cell death. Therefore, current researches

focuses on the development of treatment method, which is known as ROS-producing approach that utilizes the increased ROS level in tumor cell to death threshold, thus triggering apoptosis of tumor cell (Wang and Yi, 2008). Figure 2.5 explains the ROS threshold concept mentioned above.

Currently, the application of photo-catalyst in cancer cell treatment grabs the attention from researchers as photo-catalyst is able to produce ROS via the photo-generated of electrons and holes pairs. Most commonly applied photo-catalyst in the studies of cancer cell treatments are titanium oxide and zinc oxide. The photo-catalyst are either being used alone in the cancer cell treatment or being bio-conjugated with antibody to enhance the treatment efficiency (Xu et al., 2007).

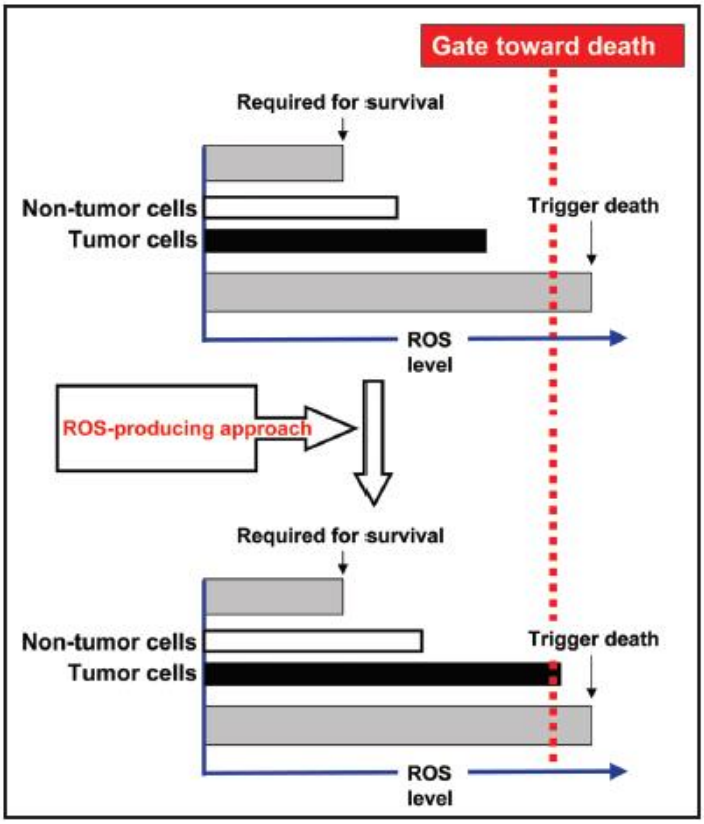

Figure 2.5: ROS Threshold in Tumor and Non-Tumor cell. (Wang and Yi, 2008)

2.6 Research Findings on Application of Photo-catalyst on Cancer Cell Treatment

According to the studies done by Abdulla-Al-Mamun, Kusumoto and Islam (2012), they evaluated the photo-catalytic performance of Ag@Fe-doped TiO2 catalyst against human epithelial carcinoma cells. They claimed that the amount of cancer cells killed was 100 % with 10 min light irradiation by using a xenom lamp as the light source. Furthermore, the viability of cancer cells was 95-100 % with the absence of light, indicating the roles of photo-catalyst in cancer cell killing. The authors further investigated the roles of light illumination in their research by conducting the research under dark conditions with the absence of light illumination. It is found that there were no observed cell killing effect, most of the cells were found to be viable. This experiment acts as a strong support on the effect of light illumination on the application of photo-catalyst. Besides, this experiment also provide strong evidence on the toxicity effect of photo-catalyst. In order to verify the contribution of ROS towards the cancer cell killing effect, the authors determine the existence of ROS produced during the treatment by employing photoluminescence technique. It is a technique that used to investigate the species exists in the sample by determining fluorescence intensity of the particular species. The authors claimed that the intensity of the photoluminescence peak is in proportion to the amount of OH· radicals produce and has good agreement with the result of the experiment where the sample which has the strongest photoluminescence peak has the best performance on cancer cell treatment.

On the other hand, Kleinsasser, Hagen and Burghartz (2010) did a research studies on the performance of zinc oxide towards human head and neck squamous cell carcinoma cell lines. It can be concluded that zinc oxide performed optimally with the condition of 0.2 and 2 µg/mL in combination of 15 min of UVA irradiation. As a compared and to investigate the cytotoxicity of zinc oxide nanoparticles towards non-tumor cells, the authors tested the effect of zinc oxide nanoparticles on primary oral mucosa cells as well. There were no cell killing effect observed in primary oral mucosa cell line below the concentration of 20 µg/mL of zinc oxide particles under UVA irradiation. Thus, the authors concluded that zinc oxide nanoparticles are able to selectively induce cancer cell death without affecting

the normal cell lines. In addition, the authors suggested to employ zinc oxide nanoparticles in photodynamic therapy, which is a new technology in cancer treatment.

CHAPTER 3

METHODOLOGY

3.1 Introduction

In this chapter, all the methods adopted in this project is clearly described from preparation to analysis of results. Sections that being discussed in this chapter are the material and equipment used, catalyst characterization method, preparation method, experimental method and analysis method. Figure 3.1 shows the flowchart of this research from preparation method analysis of result.

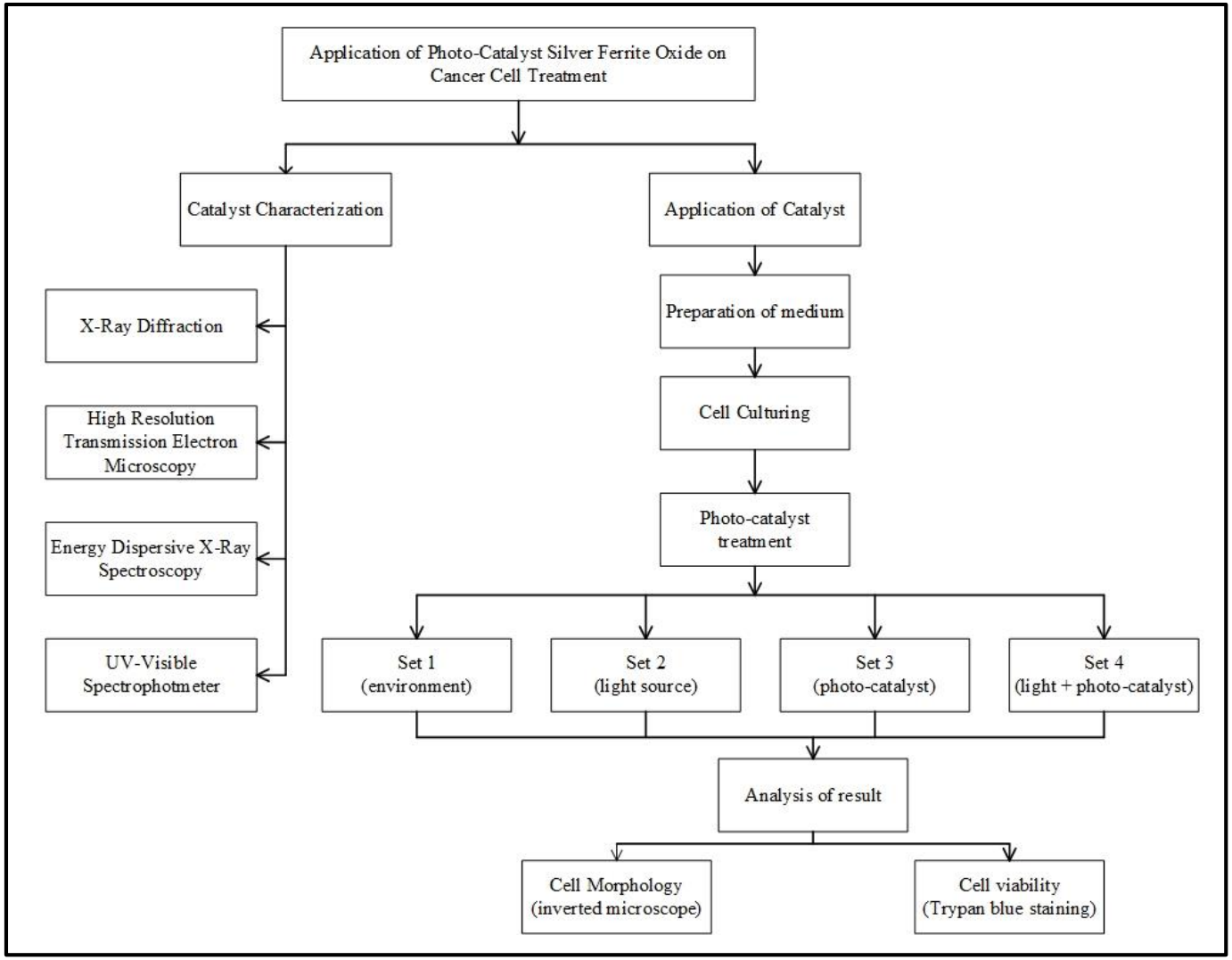

Figure 3.1: Flow Chart of Research.

3.2 Materials and Equipment Used

Materials used throughout the project is listed as below:

- 0.25 % Trypsin-EDTA solution (Sigma Aldrich)
- 90 % ethanol solution
- Fetal Bovine Serum, FBS (Biowest)
- HeLa cell line (Department of Biomedical Engineering, Universiti Tunku Abdul Rahman, Malaysia)
- Penicillin (Millipore)
- Phosphate buffered saline, PBS (Amresco)
- RPMI 1640 medium (Matrioux (M) SDN BHD)
- Silver ferrite oxide powder, $Ag_2Fe_2O_4$ (Department of Chemical Engineering, National Tsing Hwa University, Taiwan)
- Sodium hydrogen carbonate
- Trypan blue (BioWhittaker)

Equipment used throughout the project is listed as below:

- Autoclave machine (Hirayama)
- Biosafety cabinet (Telstar)
- CO_2 incubator (Heal Force)
- Drying oven
- Haemocytometer
- High Resolution Transmitting Electron Microscopy (JEOL, JEM-300F, 300 kV)
- Inverted Microscope (Olympus CKX41)
- Energy Dispersive X-ray Spectroscopy (JEOL JSM-5600 Oxford 6857)
- Ultra-sonicator (Fisher Scientific)
- UV transilluminator
- UV-Visible Spectroscopy (Hitachi U-3300)

- Water bath (Memmert)
- Weight balance
- X-Ray Diffraction (MAC Science MXP18)

3.3 Characterization of Catalyst

This section includes the following:

- X-Ray Diffraction
- High Resolution Transmission Electron Microscopy
- Energy Dispersive X-Ray Spectroscopy
- UV-Visible Spectrophotometer

3.3.1 X-Ray Diffraction (XRD)

X-Ray diffraction is a very common applied technique for catalyst characterization. XRD is operated based on X-ray diffraction on crystalline substances as crystalline plane could reflect the X-Ray beam hitting on it. Every element has different diffractive angle, therefore, XRD is commonly used in compound identification (Hull, 1919). The function of XRD are:

- Compound identification by comparing the sample's diffraction patterns with the Joint Committee of Powder Diffraction Standards (JCPDS) standard database;
- Determination of particle size by using Scherrer equation;
- Determination of d-spacing (lattice spacing) by using Bragg relation;
- Determination of crystallographic phases present in sample.

Scherrer equation is used to determine the crystallite size as following equation (Chorkendorff and Niemantsverdriet, 2003):

$$L = \frac{K\lambda}{\beta_{hkl} \cos \theta_{hkl}} \quad (3.1)$$

where

L = Crystallite size at (h k l) plane

K = Constant (often taken as 1)

λ = X-ray wavelength of radiation for CuKα

β_{hkl} = Full width at half maximum (FMHW) at (h k l) plane

$cos\ \theta_{hkl}$ = Diffraction angle at (h k l) plane in radian

The powder samples were packed into a sample holder tightly before installed in the XRD machine. The samples were scanned in a range 20 ° to 80 ° with scanning rate of 0.2 °/min. The data generated from XRD was extracted and plotted as intensity versus diffraction angle by using *Origin Pro 8.5*.

3.3.2 High Resolution Transmission Electron Spectroscopy (HRTEM)

A high resolution transmission electron spectroscopy is a microscopy technique that utilize the electron beams to provide morphologic, compositional and crystallographic information on samples. In TEM, a primary electron beam oh high energy and high intensity passes through condenser to produce parallel rays that impinge on the sample. The transmitted electrons form a two-dimensional projection of the sample mass. Therefore, one can determine the sample particle size and inter-layer spacing of catalyst at correspond diffraction plane from the HRTEM image (Chorkendorff and Niemantsverdriet, 2003).

Figure 3.2: HRTEM (JEOL, JEM-3000F, 300 kV).

3.3.3 Energy Dispersive X-Ray Spectroscopy

Energy dispersive X-Ray Spectroscopy is commonly applied in elemental analysis and it can analyze samples up to nanometer in diameter. The actual composition of sample can be determined by using EDX. The determination are in terms of weight percentage and mole percentage. EDX X-ray detector measure the intensities emitted from the sample which reflecting the distribution (EDX mapping) and composition of sample (Somorjai and Li, 2010).

In order to carry out this elemental analysis, powder sample was added to a 95 % ethanol and sonicated to give a solution with even dispersion. The solution was then dropped on a silicon buffer surface and dried. The sample was then mounted to a round holder and prior to analysis, the sample was coated with platinum to provide a path for the incident electron to flow to the ground.

3.3.4 UV-Visible Spectroscopy

The bandgap energy of semiconductor can be determined by using UV-Visible Spectroscopy. Bandgap energy is determined by applying the formula below:

$$E_G = \frac{1240}{\lambda} \tag{3.2}$$

where

E_G = Bandgap energy

λ = Cut-off wavelength.

Cut-off wavelength can be determined from the UV-Vis spectrum where the cut-off wavelength is the extended tangent line of the spectrum.

Appropriate amount of catalyst powder was added to 10 mL of distilled water. Prior to the analysis, solution was sonicated to ensure the sample catalyst were evenly distributed in the solution. 2 mL of solution was transferred to cuvette for analysis purpose. The sample was scanned from 400 nm to 800 nm with scanning rate of 100 nm/min. The data generated from UV-Vis Spectroscopy was extracted and plotted as absorbance versus wavelength by using *Origin Pro 8.5* to determine the cut-off wavelength.

3.4 Preparation Method

This section includes the following:

- Preparation of complete medium
- Cell culture
- Subculture of adherent cell (HeLa cell line and U-2 OS cell line)
- Subculture of suspended cell (Raji cell line)

3.4.1 Preparation of Complete Medium

Prior to the preparation of stock solution, both the 1 L and 250 mL Schott bottle were sterilized by using an autoclave machine with operating condition of 120 °C for 20 minutes and put into a drying oven overnight for drying purpose.

RPMI stock was prepared by adding 10.14 g of RPMI powder to distilled water with final volume of 1 L. Distilled water was added to the RPMI powder into a plastic beaker slowly to ensure the powder dissolved completely. The original packet was rinsed with little amount of distilled water to remove all traces of powder and added to the solution mentioned above. Approximately 2 g of sodium hydrogen carbonate powder was added to the solution and stirred gently to dissolve all the powder. Additional distilled water was added to bring the final volume to 1 L. The final solution was transferred into a sterilized Schott bottle after filtration using a membrane with porosity of 0.22 microns to remove any impurities. The Schott bottle was sealed with Parafilm to prevent any contamination and kept into a refrigerator operated at temperature of 4 °C.

Upon the preparation of RPMI stock solution, 225 mL of the solution was transferred to an autoclaved 250 mL Schott bottle. It was then followed by the addition of 25 mL of FBS (10 % to the complete medium) and 2.5 mL of penicillin (1 % to the

complete medium). The final solution was called complete medium and acts as the medium of the culturing cell. Penicillin was added to reduce the chances of microbial contamination in cell culture while FBS acts as the nutrient source of the cancer cells.

Figure 3.3: Complete Medium in Scott Bottle Sealed with Parafilm.

3.4.2 Preparation of Catalyst Medium

Desired amount of $Ag_2Fe_2O_4$ was weighed and mixed well with the complete medium to reach the desired concentration of catalyst medium. The concentration of $Ag_2Fe_2O_4$, denoted as *M* was computed by the following equation:

$$M = \frac{Mass\ of\ Ag_2Fe_2O_4\ (\mu g)}{Volume\ of\ complete\ medium\ (mL)} \qquad (3.1).$$

A concentrated catalyst medium was prepared and diluted to the desired concentration by applying Equation 3.2. Dilution method was used to prepare the catalyst medium as measuring the sample in micro scale may lead to inaccuracy.

$$M_1V_1 = M_2V_2 \quad (3.2)$$

where

M_1 = Concentration of the concentrated stock solution, µg/mL

V_1 = Volume of the concentrated stock solution, mL

M_2 = Concentration of the diluted solution, µg/mL

V_2 = Volume of the diluted solution, mL.

Figure 3.4 shows the catalyst medium in three different concentrations and it shows the colour of the medium deepens as the concentration increases.

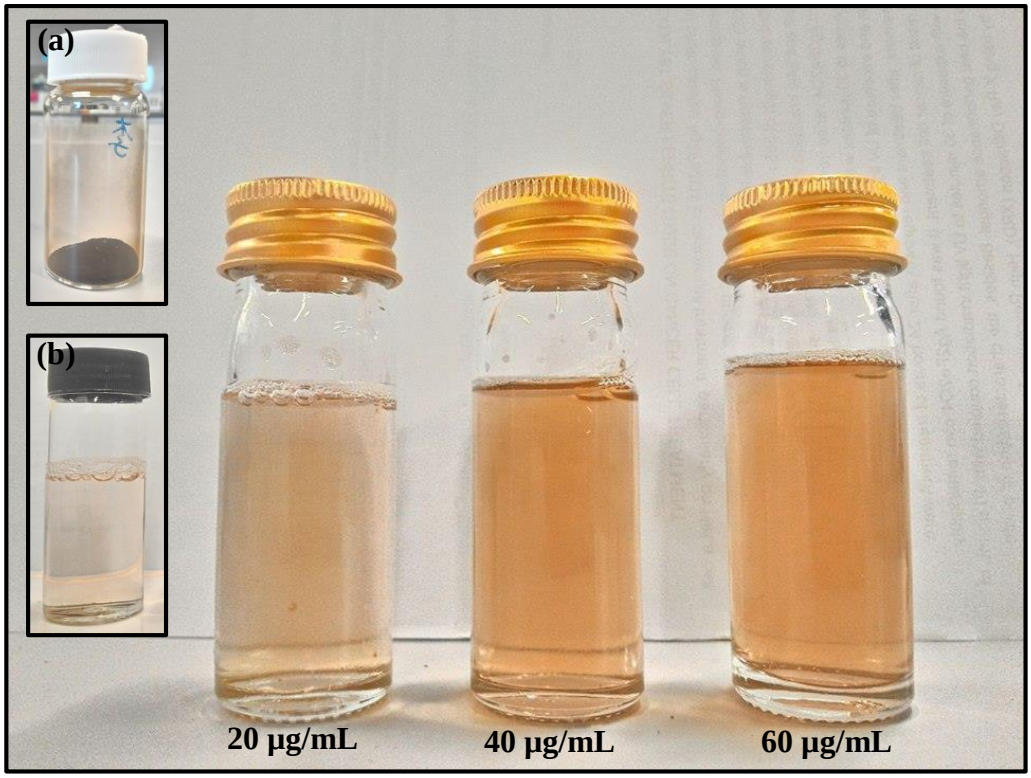

Figure 3.4: Different Concentration of Catalyst Medium. Inset (a): Black Colour of $Ag_2Fe_2O_4$ Photo-Catalyst Powder. Inset (b): 0 µg/mL of Catalyst Medium.

3.4.3 Cell Culturing

Prior to the thawing of cells, 9 mL of complete medium was transferred to a T-flask and pre-warmed in a CO_2 incubator with atmosphere of 37 °C and 5 % CO_2. Frozen cells were collected from liquid nitrogen storage by wearing appropriate protective equipment. The frozen cell was quickly thawed for 1-2 minutes with constant agitation. After the frozen cells were completely melt into liquid, the vial was wipe with 70 % ethanol before transferring into the biosafety cabinet.

Slowly drop by drop, the cells were diluted to the pre-warmed complete medium. T-flask was rinsed by the solution of cells and medium several times to ensure and enhance the mixing of cells and medium. The T-flask was put into the CO_2 incubator with atmosphere of 37 °C and 5 % CO_2. Complete medium was changed on the next day and cells were observed under an inverted microscope. The complete medium was changed every two days before all the nutrients in the media are exhausted to prevent the dying of cells.

3.4.4 Subculture of HeLa Cell Line (Adherent Cell Line)

When the surface area available of the T-flask was fully covered by the adherent cell line, sub-culturing is necessary to prevent the culture from dying. Adherent cell lines need to be brought into suspension before sub-culturing. The degree of adhesion varies with the types of cell line.

The culture was examined under an inverted microscope from time to time to check the confluency. The spent medium was discarded and 3 mL of PBS was added to the culture in order to wash away the residue of serum. Wash solution was removed and discarded and 2 mL of 0.25 % Trypsin-EDTA solution was added to the washed culture. The flask was rotated to cover the entire surface with trypsin. Trypsin was used to

detach the cell from the surface area of the flask and allow them to suspend in the liquid medium. The culture was observed under an inverted microscope, when almost 90 % of the cells were detached and floating, 7 mL of pre-warmed complete medium was added to the culture to inhibit trypsinization as prolonged exposure of trypsin to the cells may lead to the damage of cell surface receptors.

Required amount of cells were transferred to new T-flask and pre-warmed complete medium was added to reach a final volume of 10 mL. The sub-culture cell line was incubated with the atmosphere of 37 °C and 5 % CO2 in the air. Medium was changed every two days and the cells were examined under inverted microscope from time to time to confirm the absence of bacterial and fungal contaminants.

*** Note: All of the above mentioned procedures were completed in a biosafety cabinet with vertical laminar air flow and all the apparatus used were prior to UV illumination for sterilization purpose. Before beginning, the safety hood were sprayed with 70 % ethanol and wiped clean. The materials used were pre-warmed by water bath to a temperature of 37.5 °C. All the materials and apparatus were rinsed with bleach before disposing.*

3.5 Cancer Cell Treatment

The parameters of this project were the concentration of $Ag_2Fe_2O_4$ catalyst, the duration of light irradiation and the presence of a constant light source. The concentrations of $Ag_2Fe_2O_4$ were 0, 20 µg/mL, 40 µg/mL and 60 µg/mL respectively while the durations of light irradiation were 5 min, 10 min, 15 min, 20 min, 25 min and 30 min respectively. The light source that employed in this project was an UV transilluminator, which emitting light with a wavelength of 365 nm, indicated in Figure 3.5. The light treatment was carried out under room temperature. There were three groups of experimental settings. The first group was treated with different concentration of catalyst in absence

of the light source. The second group was treated with catalyst in presence of light source while the third group was irradiated in the absence of catalyst. Table 3.1 describes the setting of the three sets of experiment parameter.

Figure 3.5: UV-Transilluminator.

Table 3.1: Setting of Experiment.

Experiment	Light	Concentration of Catalyst
1	×	×
2	×	√ (Concentration/µg/mL: 20, 40, 60)
3	√ (Duration/min: 5, 10, 15,	√ (Concentration/µg/mL: 20, 40, 60)

	20, 25, 30)		
		√	
4	(Duration/min: 5, 10, 15,		×
	20, 25, 30)		

Prior to the catalyst treatment, the cells were examined under an inverted microscope to ensure the confluence of the cells and the initial morphology of the cancer cells were captured with the magnification of 10×.

In a typical catalyst treatment experiment, the old culture medium was discarded and washed with PBS solution several times to eliminate any residue medium. It was then replaced with the prepared catalyst medium, following with the incubation at standard condition (37 °C and 5 % CO_2 in air) for 48 hours. After 48 hours of incubation, the culture was irradiated with UV light with respective time duration. The effect of the treatment was investigated and evaluated after the light irradiation. For experiments with group one setting, the samples were investigated and evaluated after the incubation of 48 hours.

The catalyst medium was discarded after the treatment, fresh culture medium was added to the tested cell line and incubated for another 24 hours and the same analysis was done to evaluate the regrowth of the survivor cell line after the treatment. To investigate and evaluate the cytotoxicity, every set of experiment setting was compared with a controlled experiment. The experiments were repeated three times to improve the accuracy of result.

3.6 Analysis Method

This section includes the following:

- Morphology
- Cell Viability (Trypan blue staining)

3.6.1 Morphology of Cancer Cell

The morphology of the cancer cell was compared before catalyst treatment, after the catalyst treatment and after 24 hours of regrowth. The images were taken using an inverted Olympus CKX41 microscope as indicated in Figure 3.6. The inverted microscope consists of a numerical light field condenser to deliver a beam of white light from tungsten lamp from the top of the sample. A 10× magnification objective lens was used to observe the samples.

Figure 3.6: Inverted Olympus CKX41 Microscope.

3.6.2 Cell Viability (Trypan Blue Staining)

The most common used method to determine the cell viability is the trypan blue staining method. Trypan blue is a stain which is impermeable to living cell membrane, only enters cell with compromised membrane, which is the dead cell. Therefore, trypan blue staining method provides a direct quantitative result towards the cell viability. Trypan blue forms dye aggregates and crystals naturally, hence, it is recommended to filter the trypan blue with 0.2 μm filter prior to use. When a cell suspension is diluted with trypan blue, viable cell stays small, round and refractile whereas dead cell becomes swollen, larger and dark blue as it is stained by trypan blue (Doyle and Griffiths, 2000).

A haemocytometer is a specimen slide that used to determine the concentration of cell in a liquid suspension as well as to investigate the cell viability of a cell suspension. In other words, a haemocytometer is used to perform cell count. Before using the haemocytometer, the harmocytometer as well as the cover-slip was wiped and cleaned with 70 % ethanol. The depth of a haemocytometer is 0.1 mm, and each square of haemocytometer, which is known as chamber, represents a total volume of 0.1 mm^3. A haemocytometer consists of nine chambers in total and four out of nine are the counting chambers. The four counting chambers are located at the four corners of the haemocytometer.

Prior to the determination of cell viability, the samples required to go through trypsinization by adding appropriate amount of 0.25 % Trypsin-EDTA solution into the sample. The liquid suspension was prepared by mixing appropriate amount of trypsinized cell sample and trypan blue in PBS. A pipette was used to transfer the cell-liquid suspension into the counting chamber and covered with the cover-slip. The number of viable cell was counted in the four 1 mm^2 counting chambers. The rules of thumb during cell count is that the cells in the left-hand and top grid markings should be included in a chamber and those in the right-hand and bottom markings should be excluded as shown in Figure 3.6. The cell viability was calculated as the number of unstained cell (viable cell) against total number of cells, as indicated in the formula 3.1.

$$Viability = \frac{number\ of\ viable\ cells}{number\ of\ total\ cells} \times 100\ \% \qquad (3.3)$$

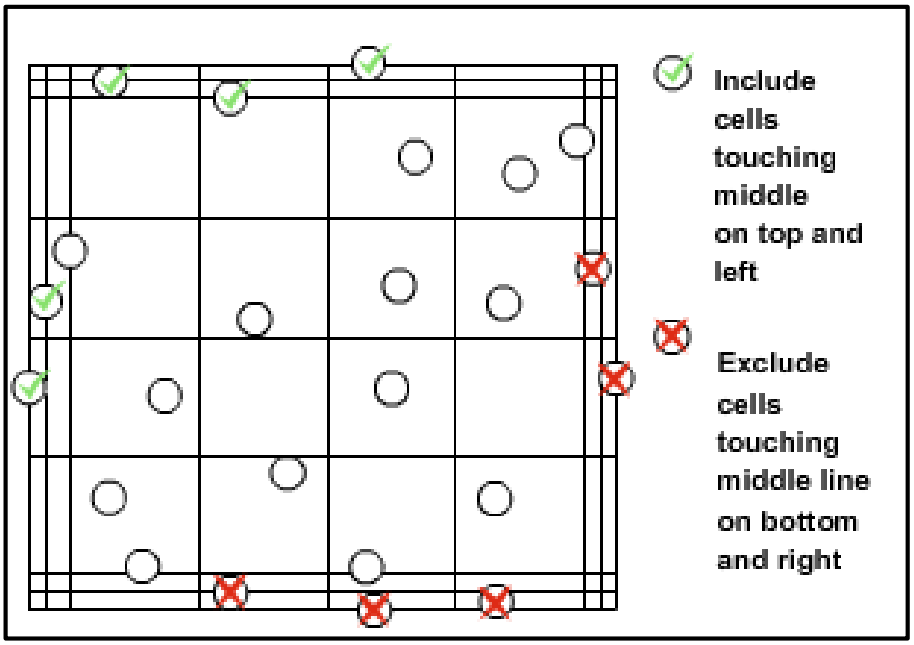

Figure 3.7: Diagram Indicating which Cells are to be Counted. (Doyle and Griffiths, 2000)

The determination of cell viability by using tyrpan blue staining method have to be completed as fast as possible, ideally within an hour as prolonged exposure of cells to trypan blue will lead to inaccuracy of results. This is because long exposure to trypan blue allows the permeability of the dye to the viable cells, which affect the accuracy of result.

CHAPTER 4

RESULTS AND DISCUSSION

4.1 Characterization of Photo-catalyst $Ag_2Fe_2O_4$

The characterization of photo-catalyst includes the particle crystallite size, morphology, composition and band gap energy. The details of each of the characterization results are discussed in the following section.

4.1.1 X-Ray Diffraction (XRD) Pattern and Grain size of Photo-Catalyst $Ag_2Fe_2O_4$

The XRD pattern of the photo-catalyst $Ag_2Fe_2O_4$ with database standard JCPDS 02-1018 and JCPDS 04-0783 are illustrated in Figure 4.1. Database JCPDS 02-1018 and JCPDS 04-0783 are used for comparison purpose for compound identification, the former is the standard of $Ag_2Fe_2O_4$ while the latter is the standard of Ag. As shown in Figure 4.1, the five major diffraction peaks of photo-catalyst sample $Ag_2Fe_2O_4$ at 28.42 °, 34.78 °, 60.96 °, 68.5 °, 72.74 °, are in good agreement with the standard JCPDS 02-1018. Furthermore, as compared to the standard JCPDS 04-0783, the diffraction peak at 38.1 ° and 77.4 ° of sample $Ag_2Fe_2O_4$ are found to be the diffraction peaks of Ag as it fitted well with the standard database. There are two symbols, black dot and black diamond are used for indication purpose, and the former indicating diffraction peaks of Ag while the latter indicating $Ag_2Fe_2O_4$. .

Since there is no extra diffraction peaks are identified, hence, it can be concluded that there are only $Ag_2Fe_2O_4$ and Ag in the photo-catalyst sample.

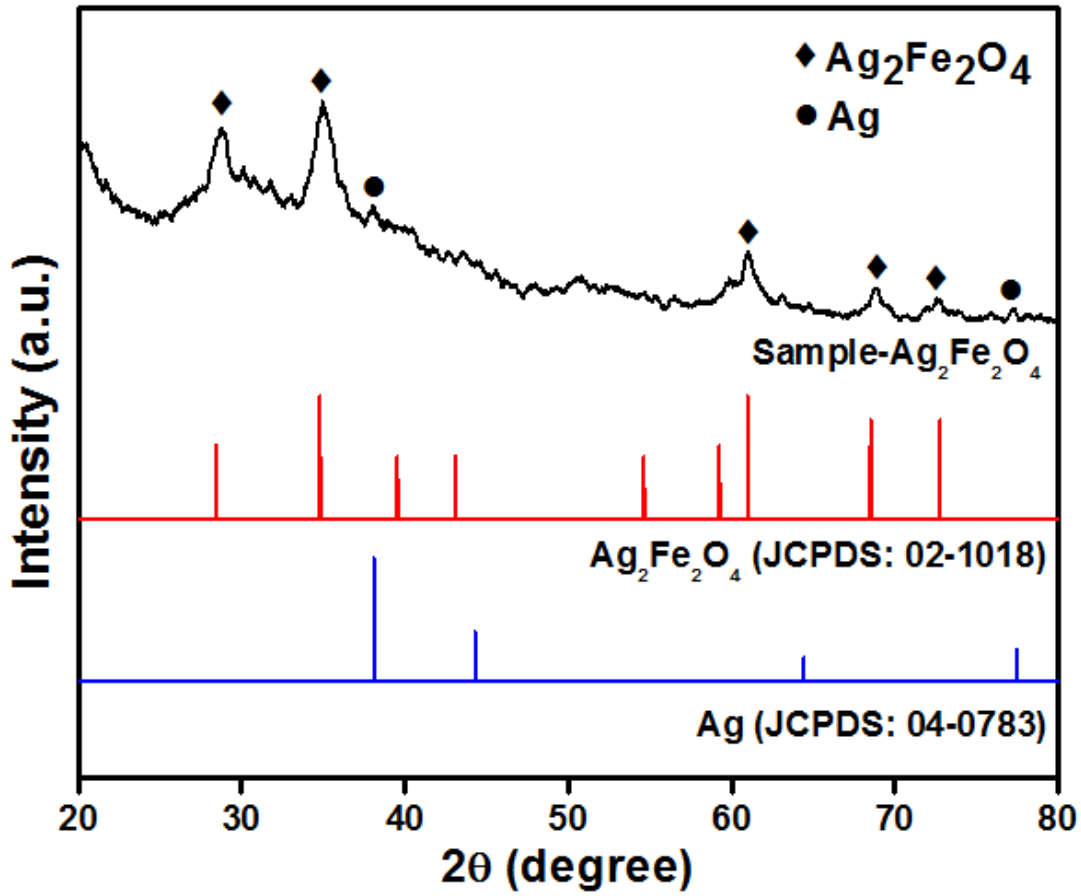

Figure 4.1: XRD Patterns of Sample $Ag_2Fe_2O_4$ and Standard Database.

In addition, the particle crystalline size can be investigated from the XRD pattern by applying Equation 3.1. The computed crystallite size is 6.7 nm with FWHM of 1.24 ° and diffraction angle of 34.87 °. The detailed calculation is attached in Appendix A.

4.1.2 High Resolution Transmission Energy Spectroscopy (HRTEM) Image and Particle Size of Photo-Catalyst $Ag_2Fe_2O_4$

The particle size of photo-catalyst $Ag_2Fe_2O_4$ is further investigated by using High Resolution Transmission Energy Spectroscopy (HRTEM). Other than that, the

crystallite lattice plan of $Ag_2Fe_2O_4$ can also be determined. Figure 4.2 shows a typical HRTEM image of $Ag_2Fe_2O_4$ while the inset is the determination of crystallite lattice plan. Twenty nanocrystals are identified and determined to give an average size of 6.5 ± 0.5 nm as indicated as the red-dashed circles in the figure. The result obtained from HRTEM is reasonably in good agreement with XRD estimation of 6.7 nm, further verify the nano scale of $Ag_2Fe_2O_4$.

The inset of Figure 4.2 shows an enlarged of HRTEM image, revealing inter-layer spacing of 0.26 nm and 0.2 nm between the (0 2 1) and (1 1 3) lattice plans respectively. The inter-layer spacing investigated are in good agreement with d-spacing of 0.258 nm and 0.21 nm of the (0 2 1) diffraction peak and (1 1 3) diffraction peaks respectively.

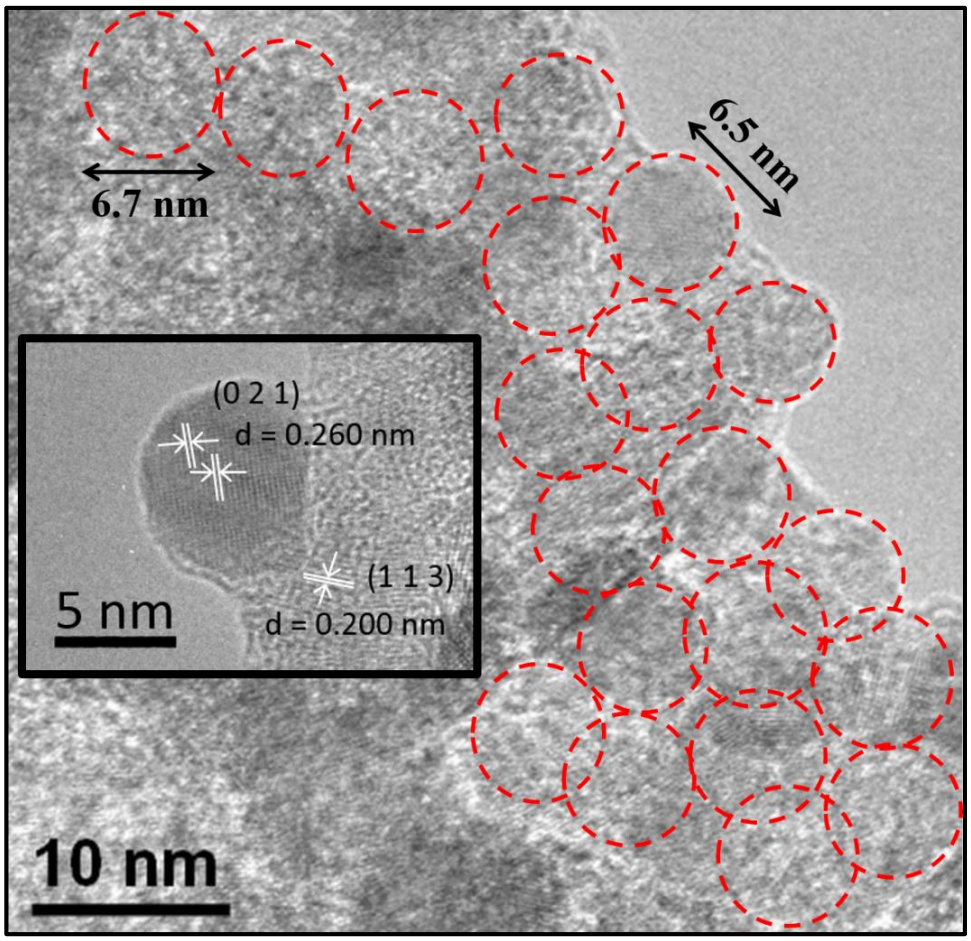

Figure 4.2: HRTEM Image of Photo-Catalyst $Ag_2Fe_2O_4$. Inset: d-spacing Determination.

4.1.3 Composition of Photo-catalyst $Ag_2Fe_2O_4$

The composition of photo-catalyst $Ag_2Fe_2O_4$ is determined by using Energy Dispersive X-ray Spectroscopy (EDX). The atomic compositions of Ag and Fe are tabulated in Table 4.2. The results shows that the ratio of Ag to Fe is around 2:2 (which is also 1:1), further confirms the composition of $Ag_2Fe_2O_4$.

Table 4.1: Atomic Composition of $Ag_2Fe_2O_4$.

Element	Atomic %	Ratio of Ag:Fe
Ag	5.79	1.1:1
Fe	5.31	

Furthermore, elemental mapping is also done by using EDX in order to study the distribution of photo-catalyst $Ag_2Fe_2O_4$. The distribution of Ag element and Fe element is shown in the inset of Figure 4.3. Both green dots and red dots in the diagram are used to indicate Ag atom and Fe atom respectively. It is obvious that Ag element and Fe element are uniformly distributed, implying a single phase of $Ag_2Fe_2O_4$ instead of separate phases of silver oxide and iron oxide.

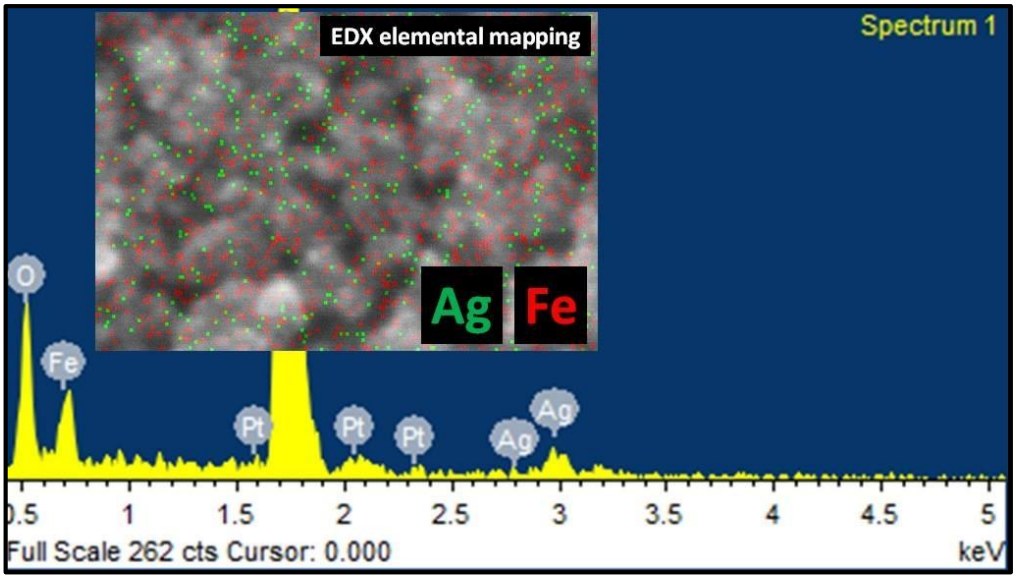

Figure 4.3: EDX Spectrum of $Ag_2Fe_2O_4$. Inset: Area Mapping of Ag and Fe Element.

4.1.4 Bandgap energy of $Ag_2Fe_2O_4$

The band gap energy of $Ag_2Fe_2O_4$ is determined from the UV-VIS absorption spectra as shown in Figure 4.4. The formula used to determine band gap energy is Formula 3.2 as discussed at Section 3.34. Bandgap energy of $Ag_2Fe_2O_4$ is found to be 2.0 eV from the UV-VIS absorption with cut-off wavelength of 620 eV. Bandgap energy plays an important roles in photocatalytic performance as it will affect the position of conduction band of photo-catalyst where the latter determines the rate of the photocatalytic in term of the generation of hydroperoxyl free radical (one type of ROS), which claimed to be involving in the destroying the cell wall and component of tumor cells (Lee et al., 2015; Castro et al., 2012).

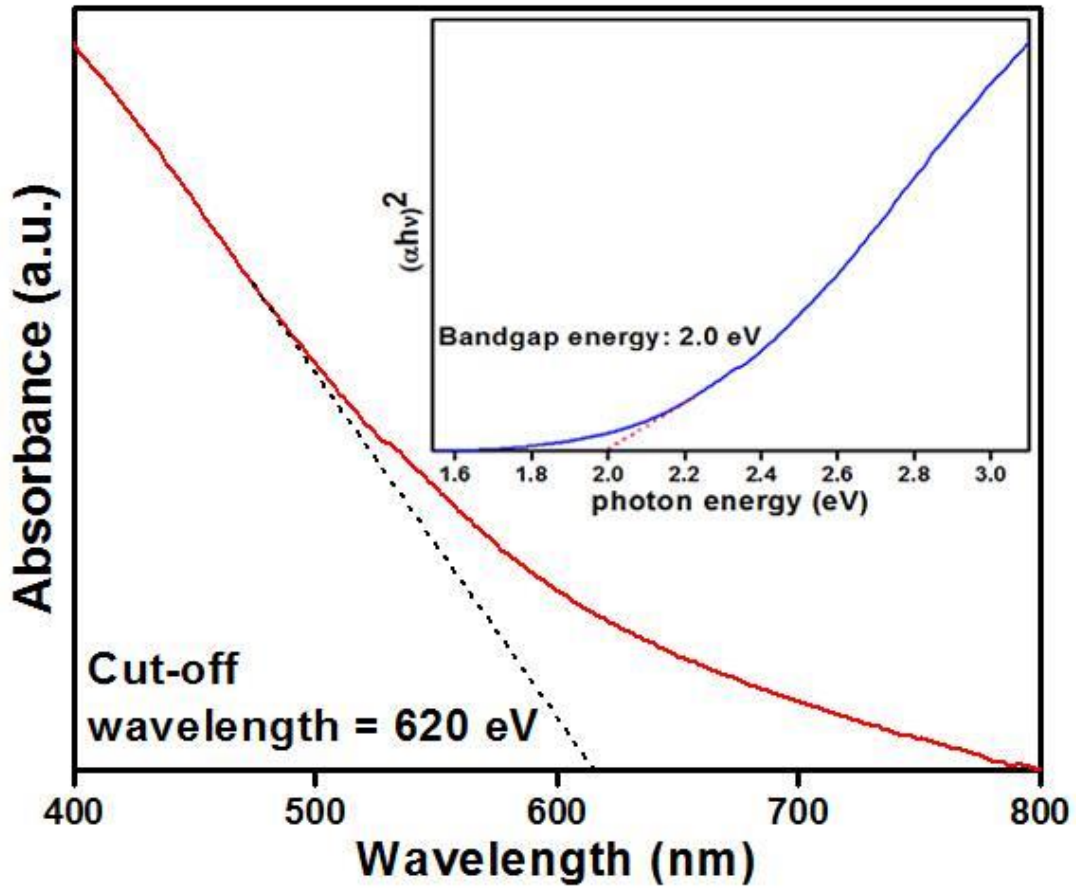

Figure 4.4: UV-Vis Adsorption Spectra of $Ag_2Fe_2O_4$. Inset: Bandgap Energy of $Ag_2Fe_2O_4$.

4.2 Application of Photo-catalyst $Ag_2Fe_2O_4$ in Cancer Cell Treatment

Photo-catalyst $Ag_2Fe_2O_4$ is applied in the cancer cell treatment, particularly HeLa cell for this project. In order to study the effect of photo-catalyst $Ag_2Fe_2O_4$ on HeLa cell, cell viability and morphology are determined. Cell viability and morphology are investigated before treatment, after treatment and after 24 hours of regrowth period. Comparison between the changes of cells in cell viability and morphology, before and after treatment gives immediate indication on the performance of photo-catalyst. The purpose of determining the properties of treated cell after 24 hours is to study the recovery of cells from photo-damage.

There are a total of four sets of experiment in this project to determine the killing effects of photo-catalyst $Ag_2Fe_2O_4$ with two parameters which are the concentration of $Ag_2Fe_2O_4$ and total irradiation time of light, as summarized in Table 4.2. An UV-transilluminator which emitted a wavelength of 365 nm is used for the light irradiation on HeLa cells.

Table 4.2: Parameters of Experiment.

Experiment	Light	Concentration of Catalyst (μg/mL)	Duration (min)
1	×	×	5, 10, 15, 20, 25, 30
2	√	×	5, 10, 15, 20, 25, 30
		20	5, 10, 15, 20, 25, 30
3	×	40	5, 10, 15, 20, 25, 30
		60	5, 10, 15, 20, 25, 30
		20	5, 10, 15, 20, 25, 30
4	√	40	5, 10, 15, 20, 25, 30
		60	5, 10, 15, 20, 25, 30

Experiment 1, 2 and 3 serve as the controlled sets of this experiment. In order to investigate the effect of the environment towards the cells, Experiment 1 is carried

out without both the parameters of light irradiation and photo-catalyst. This is because the the cells are transferred from CO_2 incubator to biosafety cabinet for preparation and treatment is carried out in UV-transilluminator, where no controlled level of CO_2 is provided to the cells. In order words, Experiment 1 serves the purpose of investigating the effect of the surrounding environment towards the cell viability within the experiment time frame. Meanwhile, Experiment 2 and Experiment 3 are to investigate the effect of light irradiation and catalyst under dark condition on cells respectively.

4.2.1 Cell Viability

Cell viability is determined as the percentage of the number of living cell against total number of cell. Trypan blue which is a dye, is used to indicate whether a cell is living. Unstained cells indicate living cells while stained cells indicate dead cells due to the rupture of cell wall and allow the entrance of dye. Figure 4.5 illustrated the difference between living cells and dead cells by using Trypan blue. The performance of photo-catalyst $Ag_2Fe_2O_4$ is explained in terms of cell viability where lower cell viability after treatment reflects better performance as more cells are inactivated.

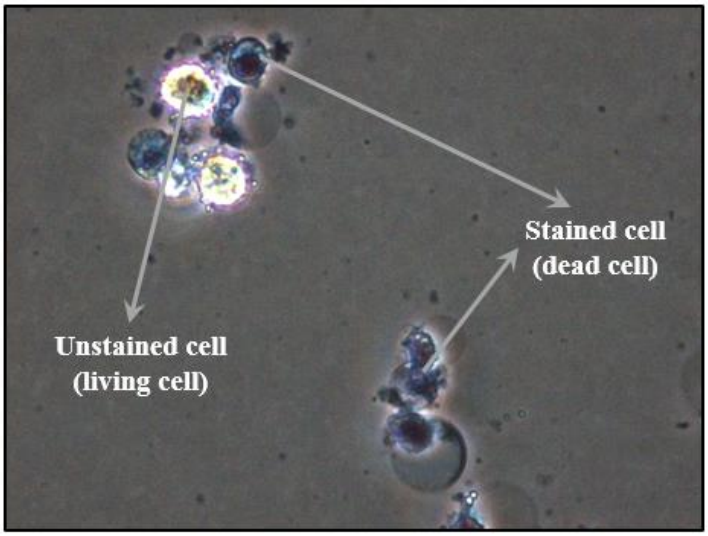

Figure 4.5: Difference between Living Cells and Dead Cells by using Trypan Blue.

The computed cell viabilities of Experiment 1, 2 and 3 are shown in Figure 4.6. The results are presented in bar chart for better illustration (enlarged version of each of the bar charts are attached in Appendix B). Columns show the mean values and standard deviation of three experiments. It shows only little reduction in cell viability for each of the experiment, indicating the experiment environment, irradiation of light on cells and exposure of photo-catalyst to cells without irradiation are not toxic for HeLa cells. The result of controlled experiment sets are in consistent with findings from Wang et al. (2013) on their study of Ag/AgCl nanostructures on photocatalytic inactivation of HeLa cells. HeLa cells was irradiated by UV light with wavelength of 360 nm from mercury lamp (Lightningcure_ L9588-01, Hamamatsu) with absence of photo-catalyst Ag/AgCl. The authors claimed that only slight decrease in viability was observed, concluded that HeLa cells were strong enough against photo-irradiation.

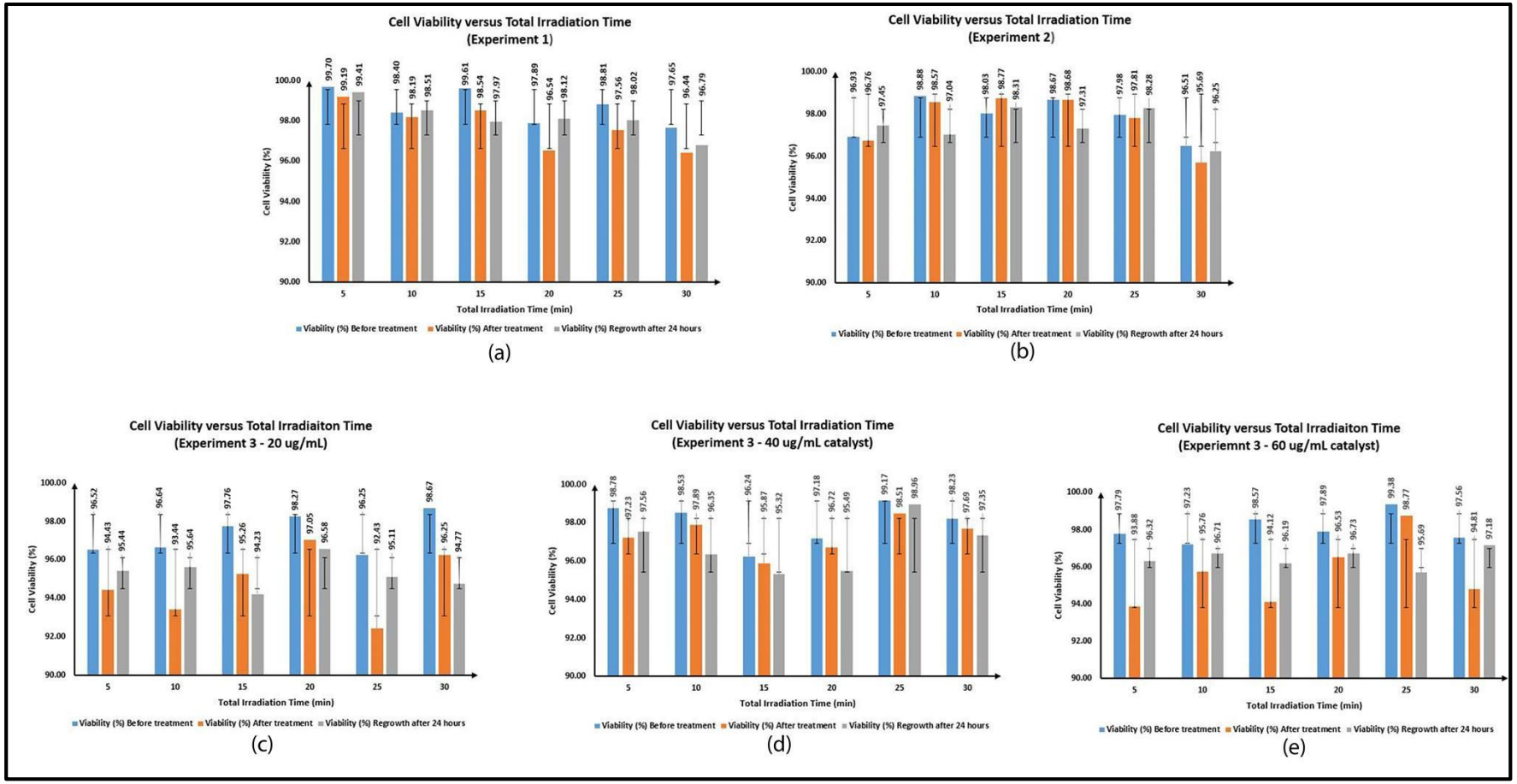

Figure 4.6: Graphs of Cell Viability versus Total Irradiation Time of (a) Experiment 1. (b) Experiment 2, (c) Experiment 3 with 20 ug/mL of $Ag_2Fe_2O_4$, (d) Experiment 3 with 40 µg/mL of $Ag_2Fe_2O_4$, (e) Experiment 3 with 60 µg/mL of $Ag_2Fe_2O_4$. Note the scale (90-100 %) of the Ordinate Instead of Ccale (0-100%).

Figure 4.7 shows the results of Experiment 4 with three different concentration of $Ag_2Fe_2O_4$ (enlarged version of each of the bar chart are attached in Appendix C). Columns show the mean values and standard deviation of three experiments. The result reveals that the combination of photo-catalyst and photo-irradiation is significant to the treatment. Photo-catalyst $Ag_2Fe_2O_4$ is photo-excited and this initiated the generation of ROS, which is responsible in the killing mechanism of cancer cell.

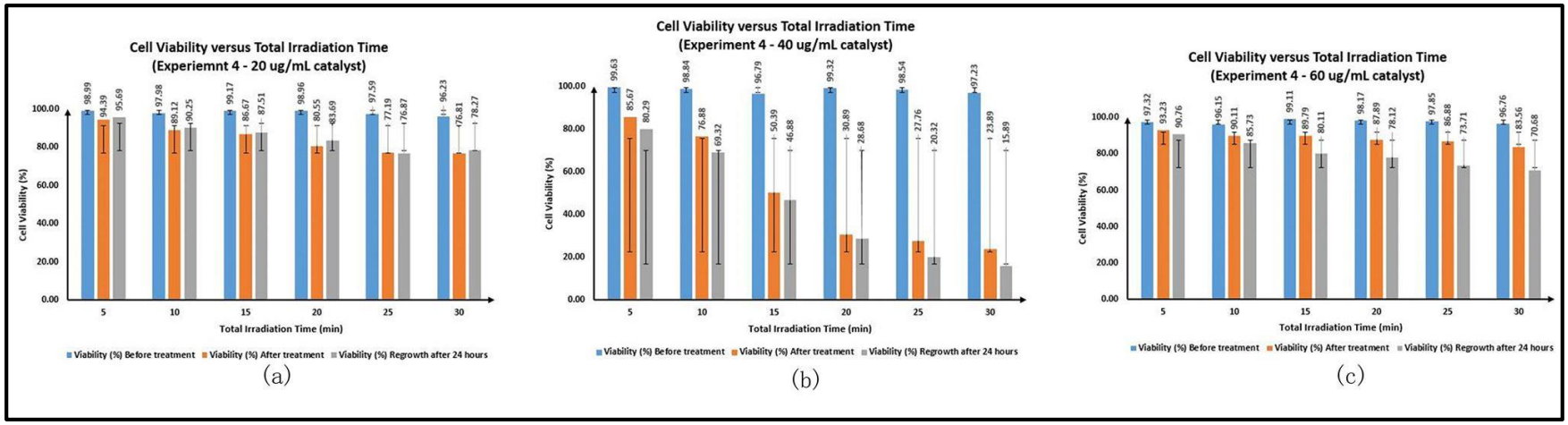

Figure 4.7: Graphs of Cell Viability versus Total Irradiation Time of Experiment 4 (a) 20 µg/mL of $Ag_2Fe_2O_4$, (b) 40 µg/mL of $Ag_2Fe_2O_4$, (c) 60 µg/mL of $Ag_2Fe_2O_4$.

The cell viability after treatment of each concentration of catalyst are plotted against total irradiation duration for better comparison as shown in Figure 4.8. Significant reduction in cell viability could be observed from the set of experiment with 40 µg/mL of $Ag_2Fe_2O_4$. Furthermore, it could be observed that treatment with three different concentrations of $Ag_2Fe_2O_4$ has the same trend, where the cell viability decreases as light irradiation time increases. In other words, more cancer cells are being inactivated with longer exposure to UV irradiation. The cell viability drops to 23.89 % after 30 minutes of treatment with 40 µg/mL of $Ag_2Fe_2O_4$.

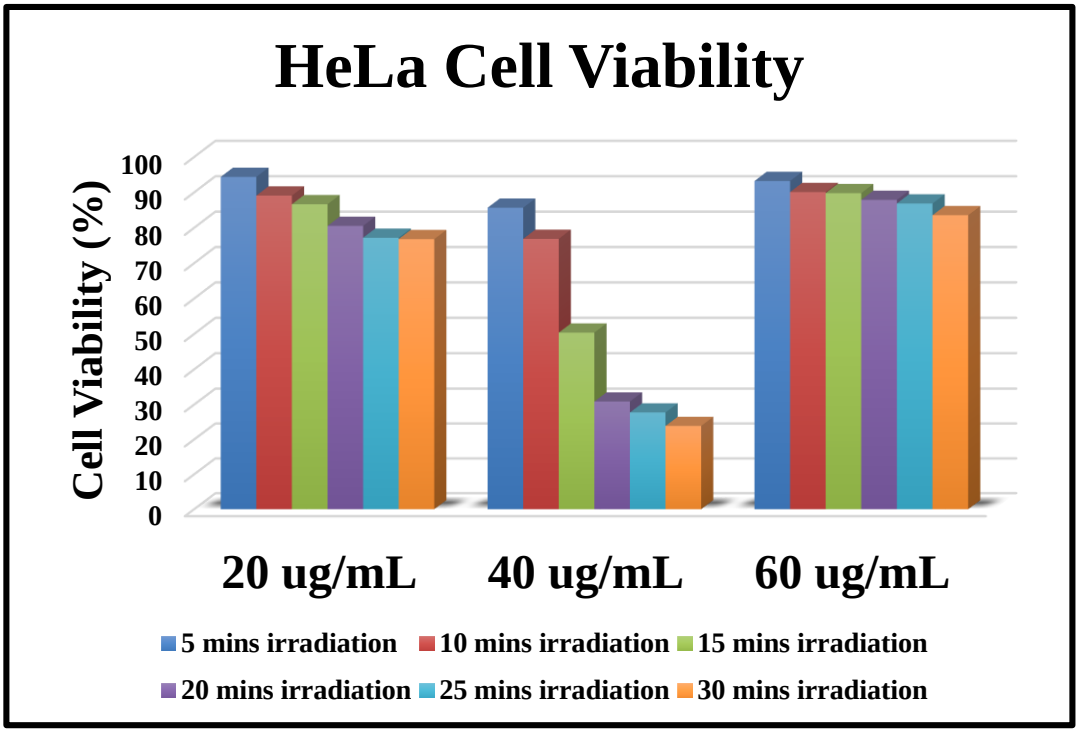

Figure 4.8: Cell Viability of HeLa Cells under UV Light i\Irradiation of 365 nm in the Presence of Different Concentration of $Ag_2Fe_2O_4$ from 20 ug/mL to 60 ug/mL.

The positive performance of $Ag_2Fe_2O_4$ with increasing time can be explained by the longer time allowance for the production of ROS. Longer time length allows more amount of ROS produced after the photo-catalysts being photo-excited by UV irradiation. Therefore, more ROS is available to involve in the destroying the cell membrane and structure of cancer cell, leading to apoptosis of cell. The nano size of $Ag_2Fe_2O_4$ contributes to the higher available total surface area for generation of ROS

to takes place. It is clear that solution with concentration of 40 µg/mL has more amount of $Ag_2Fe_2O_4$ than solution with 20 µg/mL. Hence, the former has more available total surface area for production of ROS that is responsible for cancer cell killing mechanism. It is tally with the results of solution with 40 µg/mL of $Ag_2Fe_2O_4$ performed better than solution with concentration of 20 µg/mL.

On the other hand, solution with 60 µg/mL concentration has lower catalytic performance than 40 µg/mL, where it is supposed to perform better than solution with 40 µg/mL as the latter has more amount of $Ag_2Fe_2O_4$ as compared to the former. One of the possible explanation for such phenomena might be the more-intense-aggregation of $Ag_2Fe_2O_4$ particles at higher concentration, therefore, reducing the total available surface area for generation of ROS. This statement can be verified by taking Scanning Electron Microscopy image of the three concentration of solutions and compare the aggregation extent. If the aggregation of 60 µg/mL catalyst medium happen to be more severe, then the explanation is valid.

Figure 4.9 shows the graph of cell viability after 24 hours of regrowth, which serves the purpose to study the recovery of treated cells from damage. The regrowth of treated cells after 24 hours is relatively slow, indicating the difficulty in the recovery of treated cells from photo-injury.

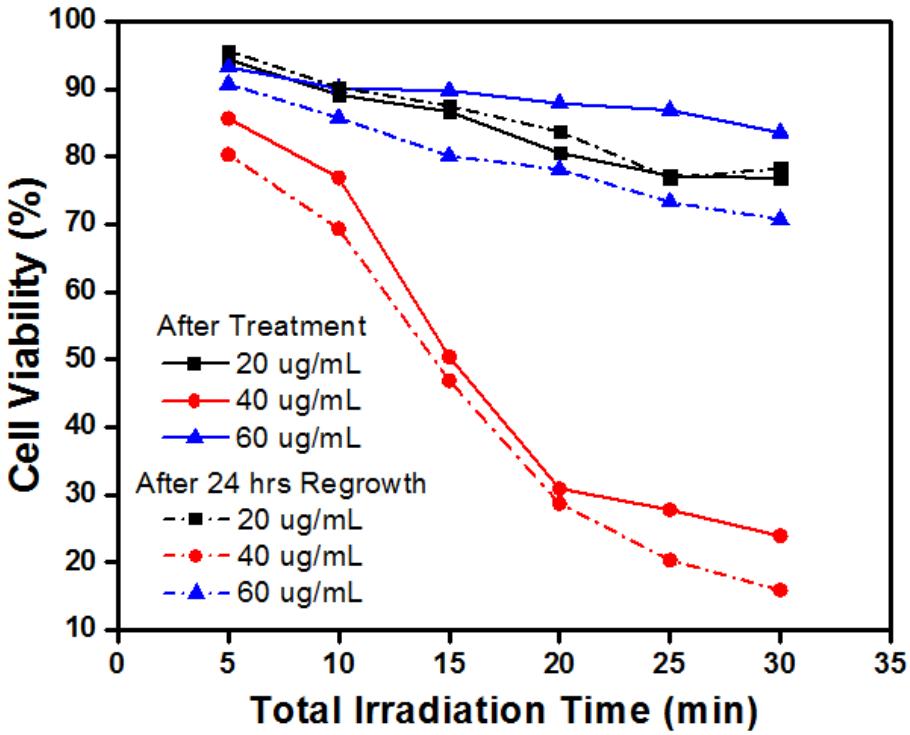

Figure 4.9: Cell Viability after 24 Hours of Regrowth of Three Different Concentration Photo-Catalyst $Ag_2Fe_2O_4$ of Treated HeLa Cells.

4.2.2 Morphology of cells

Morphology of HeLa cells is taken before treatment, after treatment and after 24 hours of regrowth. Morphology changes serves as an indication whether the cells are living. Cell confluency had to be more than 95 % before treatment, in which the cells form a complete monolayer on the wall of T-flask. If the cells are inactivated, the cells will apparently shrink and detached from the wall surface, leaving gaps between cells. Therefore, bigger gap between cells act as an indication that more cells are being inactivated. Figure 4.10 shows the difference between cells with more than 95 % confluency and less than 95 % confluency.

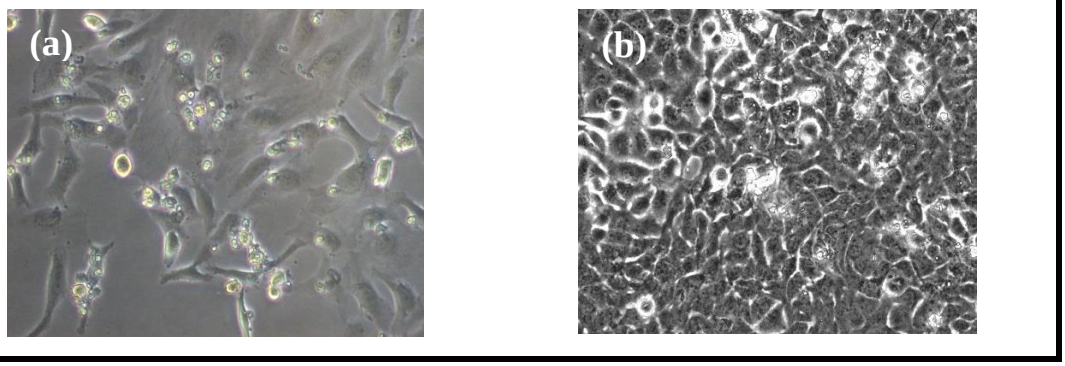

Figure 4.10: Morphology of HeLa Cells After Incubation (a) Confluency Less Than 95 %, with Gaps between Cells, (b) Confluency More Than 95 % (100 %), forming a Complete Monolayer.

Figure 4.11 shows the microscopic image of HeLa cells before treatment, after treatment and after 24 hours of regrowth of Experiment 1 with duration of 30 minutes. It can be seen that the morphology remained unchanged, indicating the cell viability remained, which is in good agreement with discussion of Section 4.2.1, where there is only little reduction in cell viability for set 1, 2 and 3.

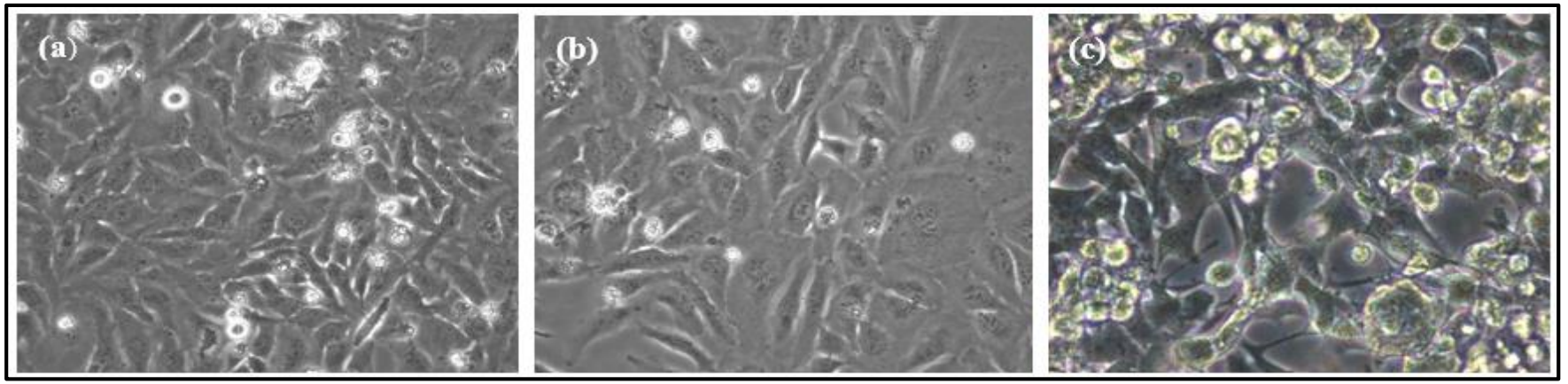

Figure 4.11: Morphology of HeLa Cells (a) Before Treatment, (b) After Treatment and (c) After 24 hours of Regrowth, with Exposure Time of 30 minutes. (Experiment 1)

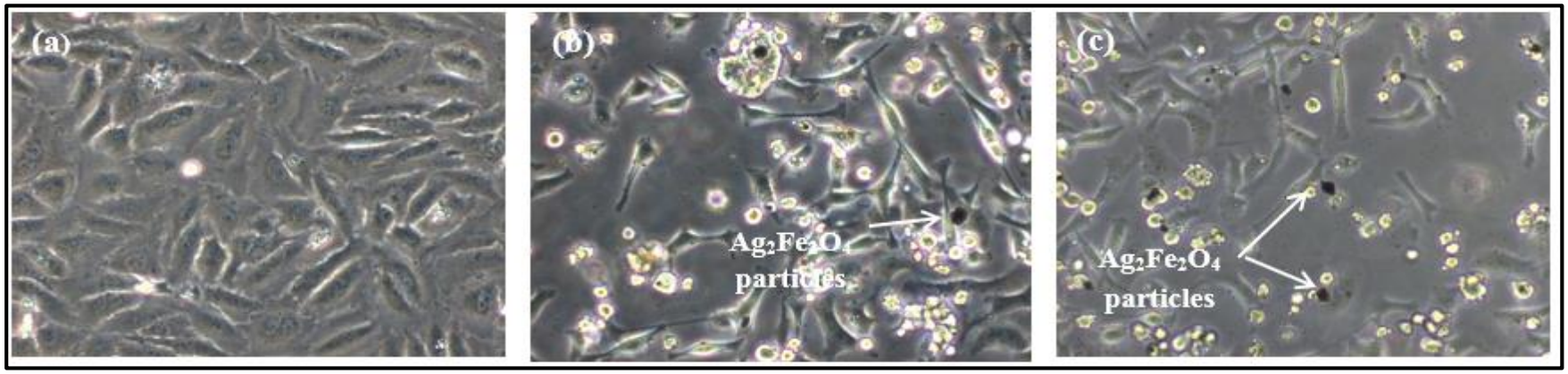

Figure 4.12: Morphology of HeLa Cells (a) Before Treatment, (b) After Treatment and (c) After 24 hours of Regrowth, with Exposure time of 30 minutes and 20 µg/mL of $Ag_2Fe_2O_4$. (Experiment 4)

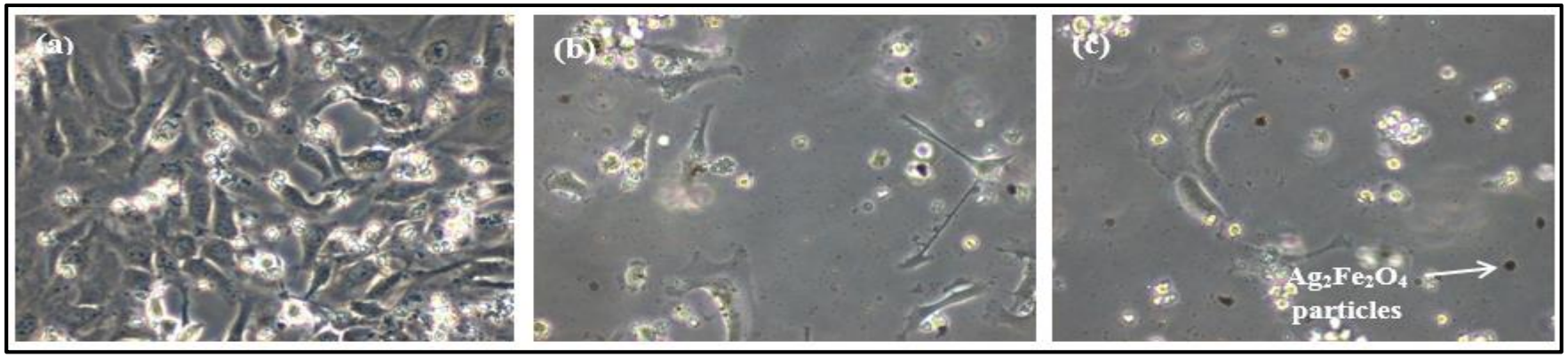

Figure 4.13: Morphology of HeLa Cells (a) Before Treatment, (b) After Treatment and (c) After 24 hours of Regrowth, with Exposure Time of 30 minutes and 40 µg/mL of $Ag_2Fe_2O_4$. (Experiment 4)

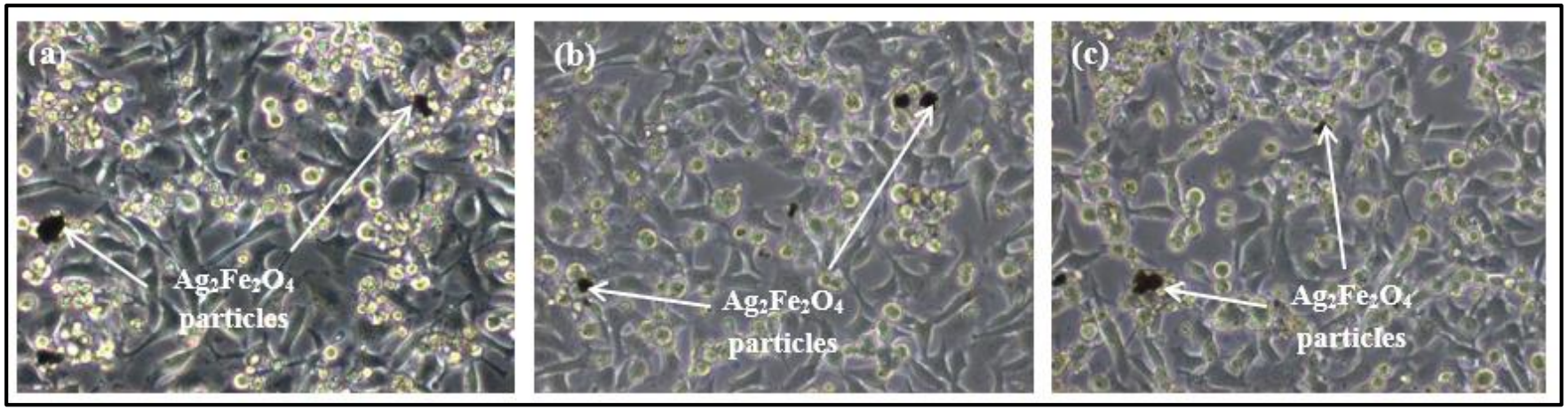

Figure 4.14: Morphology of HeLa Cells (a) Before Treatment, (b) After Treatment and (c) After 24 hours of Regrowth, with Exposure Time of 30 minutes and 60 µg/mL. (Experiment 4)

Figure 4.12 to 4.14 are the microscopic images of HeLa cells in (a) before treatment, (b) after treatment and (c) after 24 hours of regrowth with exposure time of 20 µg/mL, 40 µg/mL and 60 µg/mL of $Ag_2Fe_2O_4$ respectively. It is obviously noticed that there is changes in the morphology for three sets of experiment after treatment. Experiment set with 40 µg/mL has the largest changes, the big gap between cells indicating high percentage of cancer cells are being inactivated. The morphology after 24 hours of regrowth indicate the difficulty of cells from recovering, in consistent with the quantitative investigation at part 4.2.1.

The enlarged version of each of the HeLa cell images in Figure 4.10, 4.11, 4.12, 4.13 and 4.14 are attached in Appendix D, E, F, G and H respectively.

CHAPTER 5

CONCLUSION AND RECOMMENDATIONS

5.1 Conclusions

In the present study, X-Ray Diffraction, High Resolution Transmission Energy Spectrometry, Energy Dispersive X-ray Spectroscopy and UV-Visible Spectrophotometer were used to characterize photo-catalyst $Ag_2Fe_2O_4$. The XRD diffraction peaks and results from EDX confirmed that the sample catalyst is $Ag_2Fe_2O_4$ where the diffraction peaks of sample catalyst was compared with standard JCPDS 02-1018 for identification and the atomic ratio of Ag and Fe was determined to be 2:2 from EDX. The particle grain size was determined from XRD as well as HRTEM. The result obtained from XRD was 6.7 nm, in considerably good agreement with result of HRTEM of 6.5 ± 0.5 nm (average size of twenty determined particles). The bandgap energy of $Ag_2Fe_2O_4$ was 2.0 eV with cutoff wavelength of 620 nm, determined by using UV-Vis Spectrophotometer.

Based on the results obtained from the cancer treatment, cultured HeLa cells were effectively killed by photo-excited $Ag_2Fe_2O_4$ nano-particles *in vitro*. There were two variables affecting the photo-catalytic performance of $Ag_2Fe_2O_4$. Those were concentration of photo-catalyst and total irradiation time. It was found that apoptosis of HeLa cells was only being induced with the presence of both $Ag_2Fe_2O_4$ and UV light irradiation. This statement is supported by the results from Experiment 1, 2 and 3, where no significance reduction (reduction in the range of 0.51 % to 3.91 %) in cell viability was found. When the concentration of $Ag_2Fe_2O_4$ increased from 20 µg/mL to 40 µg/mL, the cell viability decreased significantly as total

irradiation time increased. However, when the concentration of photo-catalyst increased to 60 µg/mL, low reduction in cell viability was found. This might due to the aggregation of $Ag_2Fe_2O_4$ at high concentration. Apart from the effect of photo-catalyst concentration, the cell surviving rate decreased with longer irradiation time. The cell viability after 24 hours of regrowth was determined and the regrowth rate decreased as concentration of $Ag_2Fe_2O_4$ and irradiation time increased, indicating difficulty in the recovery of treated cells from photo-injury.

This study on the effect of photo-excited catalyst on HeLa cell treatment suggested the idea of cancer treatment using $Ag_2Fe_2O_4$ and light irradiation. Although UV light with wavelength of 365 nm cannot penetrate the human body deeply, it is believed that it may be possible to be adapted to an anticancer modality in the future where the issue on the penetration of UV light might be overcame by employing fibre optics in the transmission of UV light to the targeted cell.

5.2 Recommendations

Further investigation on the production of Reactive Oxygen Species (ROS) can be done in order to support the claim that ROS is responsible in destroying cell membrane and leading to apoptosis of cells. Photoluminescence technique using terephthalic acid as a probe molecule can be used to detect the concentration of ROS formed. The theory behind is that terephthalic acid will react with ROS to form highly fluorescent product, 2-hydrxyterephthalic. Hence, the photoluminescence peak of 2-hydrxyterephthalic at 425 nm is measured as it reflects the amount of ROS generated (Abdulla-Al-Mamun, Kusumoto and Islam, 2012).

Other than that, the position of conduction band of photo-catalyst can be determined by cyclic voltammetry analysis. The knowledge of the conduction band is significant in terms of the generation of hydroxyl free radicals from absorbed oxygen molecule and water molecule. If the conduction band of photo-catalyst is more negative than the potential of the $O_2/HO_2•$ reaction, more hydroxyl free radicals

(HO_2•) can be generated, thus, boosting the photo-catalytic performance (Lee et al., 2015).

Besides, it is suggested to apply the current experiment setting on normal healthy cell, particularly cervical cell to determine the feasibility of $Ag_2Fe_2O_4$ on the application *in vivo*. This is important as it serves the purpose of ensuring only targeted cancer cell is being inactivated without affecting the normal healthy cell.

REFERENCES

Abdulla-Al-Mamun, M., Kusumoto, Y. and Islam, M., 2012. Enhanced photocatalytic cytotoxic activity of Ag@Fe-doped TiO2 nanocomposites against human epithelial carcinoma cells. *Journal of Materials Chemistry*, 22(12), p.5460.

Alexander, J., 2009. History of the Medical Use of Silver. *Surgical Infections*, 10(3), pp.289-292.

Boonrattanakij, N., Lu, M. and Anotai, J., 2009. Kinetics and mechanism of 2,6-dimethyl-aniline degradation by hydroxyl radicals. *Journal of Hazardous Materials*, 172(2-3), pp.952-957.

Cai, R., Kubota, Y., Shium, T., Sakai, H., Hashimoto, K. and Fujishima, A., 1992. Induction of cytotoxicity by photoexcited TiO2 particles. *Cancer Res*, 52(8), pp.2346-2348.

Castro, C., Jurado, A., Sissa, D. and Giraldo, S., 2012. Performance of Ag-TiO2 Photocatalysts towards the Photocatalytic Disinfection of Water under Interior-Lighting and Solar-Simulated Light Irradiations. *International Journal of Photoenergy*, 2012, pp.1-10.

Cellresource.cn., 2009. *China Infrastructures of Cell Lines Research*. [online] Available at: http://cellresource.cn/fcellpicture.aspx?pic=PUMC%E2%80%94%E2%80%94%E4%BA%BA%E5%AE%AB%E9%A2%88%E7%99%8C%E7%BB%86%E8%83%9E%E7%B3%BB;HeLa [Accessed 3 Jul. 2015].

Chan, S., Yeong Wu, T., Juan, J. and Teh, C., 2011. Recent developments of metal oxide semiconductors as photocatalysts in advanced oxidation processes (AOPs) for treatment of dye waste-water. *J. Chem. Technol*. Biotechnol., 86(9), pp.1130-1158.

Clerkin, J., Naughton, R., Quiney, C. and Cotter, T., 2008. Mechanisms of ROS modulated cell survival during carcinogenesis. *Cancer Letters*, 266(1), pp.30-36.

Crosta, P., 2008. *Cancer: Types, Symptoms and Causes*. [online] Medicalnewstoday.com. Available at:

http://www.medicalnewstoday.com/info/cancer-oncology/ [Accessed 21 Aug. 2015].

Daniel, R., 2005. *The cancer directory*. London: Thorsons.

D'Autréaux, B. and Toledano, M., 2007. ROS as signalling molecules: mechanisms that generate specificity in ROS homeostasis. *Nature Reviews Molecular Cell Biology*, 8(10), pp.813-824.

de Boer-Dennert, M., de Wit, R., Schmitz, P., Djontono, J., v Beurden, V., Stoter, G. and Verweij, J., 1997. Patient perceptions of the side-effects of chemotherapy: the influence of 5HT3 antagonists. *Br J Cancer*, 76(8), pp.1055-1061.

Deer, W., Howie, R. and Zussman, J., 1992. *An introduction to the rock-forming minerals*. Harlow: Longman.

Diwan, B. and Murugan, S., 2013. Role of size on effective band gap in Silicon nano-solid. *International Conference on Advanced Nanomaterials & Emerging Engineering Technologies*.

Djurišić, A., Leung, Y. and Ching Ng, A., 2014. Strategies for improving the efficiency of semiconductor metal oxide photocatalysis. *Materials Horizons*, 1(4), p.400.

Doyle, A. and Griffiths, J., 2000. *Cell and tissue culture for medical research*. Chichester: Wiley.

Gomatam, R. and Mittal, K., 2008. *Electrically conductive adhesives*. Leiden: VSP.

Halliwell, B., 1991. Drug Antioxidant Effects. Drugs, 42(4), pp.569-605.

Held, P., 2015. An Introduction to Reactive Oxygen Species - Measurement of ROS in Cells. [online] *Biotek.com*. Available at: http://www.biotek.com/resources/articles/reactive-oxygen-species.html [Accessed 19 Aug. 2015].

Huang, K., Chen, L., Deng, J. and Xiong, J., 2012. Enhanced Visible-Light Photocatalytic Performance of Nanosized Anatase TiO 2 Doped with CdS Quantum Dots for Cancer-Cell Treatment. *Journal of Nanomaterials*, 2012, pp.1-12.

Jemal, A., Tiwari, R., Murray, T., Ghafoor, A., Samuels, A., Ward, E., Feuer, E. and Thun, M., 2004. Cancer Statistics, 2004. CA: *A Cancer Journal for Clinicians*, 54(1), pp.8-29.

Jiang, Z., Kun, L., Ouyang, H., Liang, A. and Jiang, H., 2011. A Simple and Sensitive Fluorescence Quenching Method for the Determination of H2O2 Using Rhodamine B and Fe3O4 Nanocatalyst. *J Fluoresc*, 21(5), pp.2015-2020.

Karpova, M., Schoumans, J., Ernberg, I., Henter, J., Nordenskjöld, M. and Fadeel, B., 2004. Raji revisited: cytogenetics of the original Burkitt's lymphoma cell line. *Leukemia*.

Kiser, M., Westerhoff, P., Benn, T., Wang, Y., Pérez-Rivera, J. and Hristovski, K., 2009. Titanium Nanomaterial Removal and Release from Wastewater Treatment Plants. *Environmental Science & Technology*, 43(17), pp.6757-6763.

Kleinsasser., 2010. Zinc oxide nanoparticles induce photocatalytic cell death in human head and neck squamous cell carcinoma cell lines in vitro. *Int J Oncol*, 37(6).

Kleinsasser, N., Hagen, R. and Burghartz, M., 2010. Zinc oxide nanoparticles induce photocatalytic cell death in human head and neck squamous cell carcinoma cell lines in vitro. *Int J Oncol*, 37(6), pp.1583-1590.

Kong, L., Jiang, Z., Xiao, T., Lu, L., Jones, M. and Edwards, P., 2011. Exceptional visible-light-driven photocatalytic activity over BiOBr–ZnFe2O4 heterojunctions. *Chemical Communications*, 47(19), p.5512.

Lee, K., Chuah, X., Cheng, Y. and Lu, S., 2015. Pt coupled ZnFe 2 O 4 nanocrystals as a breakthrough photocatalyst for Fenton-like processes – photodegradation treatments from hours to seconds. *J. Mater. Chem. A*, 3(36), pp.18578-18585.

Li, W., 2013. Photocatalysis of Oxide Semiconductors. *Journal of the Australian Ceramic Society*, 49(2), pp.41-46.

Liou, G. and Storz, P., 2010. Reactive oxygen species in cancer. *Free Radic Res*, 44(5), pp.479-496.

Miller, A., Hoogstraten, B., Staquet, M. and Winkler, A., 1981. Reporting results of cancer treatment. *Cancer*, 47(1), pp.207-214.

Mohseny, A., Machado, I., Cai, Y., Schaefer, K., Serra, M., Hogendoorn, P., Llombart-Bosch, A. and Cleton-Jansen, A., 2011. Functional characterization of osteosarcoma cell lines provides representative models to study the human disease. *Lab Invest*, 91(8), pp.1195-1205.

Qureshi, S., 2014. *Different Approaches of Cancer Treatment Using Homeopathy in Pakistan.* [online] Sabeelhomeoclinic.com. Available at: http://www.sabeelhomeoclinic.com/common-approaches-to-treat-cancer-in-homeopathy.html [Accessed 21 Aug. 2015].

Renschler, M., 2004. The emerging role of reactive oxygen species in cancer therapy. *European Journal of Cancer*, 40(13), pp.1934-1940.

Serpone, N. and Emeline, A., 2002. Suggested terms and definitions in photocatalysis and radiocatalysis. *International Journal of Photoenergy*, 4(3), pp.91-131.

Shen, K., 2013. Identification of a cancer stem cell-like side population in the HeLa human cervical carcinoma cell line. *Oncology Letters*.

Somorjai, G. and Li, Y., 2010. *Introduction to surface chemistry and catalysis*. Hoboken, N.J.: Wiley.

Sullivan, L. and Chandel, N., 2014. Mitochondrial reactive oxygen species and cancer. *Cancer Metab*, 2(1), p.17.

Townley, H., Kim, J. and Dobson, P., 2012. In vivo demonstration of enhanced radiotherapy using rare earth doped titania nanoparticles. *Nanoscale*, 4(16), pp.5043-5050.

Van Zeghbroeck, B., 2010. *Principles of semiconductor devices and heterojunctions*. Upper Saddle River, N.J.: Prentice Hall.

Viswanathan, B., Sivasanker, S. and Ramaswamy, A., 2002. *Catalysis*. New Delhi: Narosa Pub. House.

Wang, G., Mitomo, H., Matsuo, Y., Shimamoto, N., Niikura, K. and Ijiro, K., 2013. DNA-templated plasmonic Ag/AgCl nanostructures for molecular selective photocatalysis and photocatalytic inactivation of cancer cells. *Journal of Materials Chemistry B*, 1(43), p.5899.

Wang, J. and Yi, J., 2008. Cancer cell killing via ROS: To increase or decrease, that is the question. *Cancer Biology & Therapy*, 7(12), pp.1875-1884.

Waris, G. and Ahsan, H., 2006. Journal of Carcinogenesis, 5(1), p.14.

Wayu, M., King, J., Johnson, J. and Chusuei, C., 2015. A Zinc Oxide Carbon Nanotube Based Sensor for In Situ Monitoring of Hydrogen Peroxide in Swimming Pools. *Electroanalysis*, p.n/a-n/a.

Xing, M., Ge, L., Wang, M., Li, Q., Li, X. and Ouyang, J., 2014. Nanosilver particles in medical applications: synthesis, performance, and toxicity. *International Journal of Nanomedicine*, p.2399.

Xu, J., Sun, Y., Huang, J., Chen, C., Liu, G., Jiang, Y., Zhao, Y. and Jiang, Z., 2007. Photokilling cancer cells using highly cell-specific antibody–TiO2 bioconjugates and electroporation. *Bioelectrochemistry*, 71(2), pp.217-222.

Yu, T., Cheng, W., Chao, K. and Lu, S., 2013. ZnFe2O4 decorated CdS nanorods as a highly efficient, visible light responsive, photochemically stable, magnetically recyclable photocatalyst for hydrogen generation. *Nanoscale*, 5(16), p.7356.

Zhang, AP. and Sun, YP., 2004. Photocatalytic killing effect of TiO2 nanoparticles on Ls-174-t human colon carcinoma cells. *World Journal of Gastroenterology*, 10(21), pp.3191-3193.

Zhang, S., Yang, D., Jing, D., Liu, H., Liu, L., Jia, Y., Gao, M., Guo, L. and Huo, Z., 2014. Enhanced photodynamic therapy of mixed phase TiO2(B)/anatase nanofibers for killing of HeLa cells. *Nano Res*., 7(11), pp.1659-1669.

APPENDICES

APPENDIX A: Calculation of $Ag_2Fe_2O_4$ Particle Size

$$L = \frac{K\lambda}{\beta_{hkl} \cos \theta_{hkl}} \quad (3.1)$$

where

L = Crystallite size at (h k l) plane

K = Constant (often taken as 0.9)

λ = X-ray wavelength of radiation for CuKα

β_{hkl} = Full width at half maximum (FMHW) at (h k l) plane in radian

$cos\ \theta_{hkl}$ = Diffraction angle at (h k l) plane in radian

Data extracted from XRD pattern are as below:

β_{hkl} = 1.24 ° = 0.02164 rad

$cos\ \theta_{hkl}$ = $\cos\left(\frac{34.78° \times \pi}{2 \times 180°}\right) = 0.954\ rad$

Given λ as 0.154 nm, the crystallite size is therefore computed as below:

$$L = \frac{0.9 \times 0.154}{0.0216 \times 0.954}$$

$$= 6.7\ nm$$

APPENDIX B: Enlarged Bar Chart of Figure 4.6

Enlarged Bar Chart of 4.6(a).

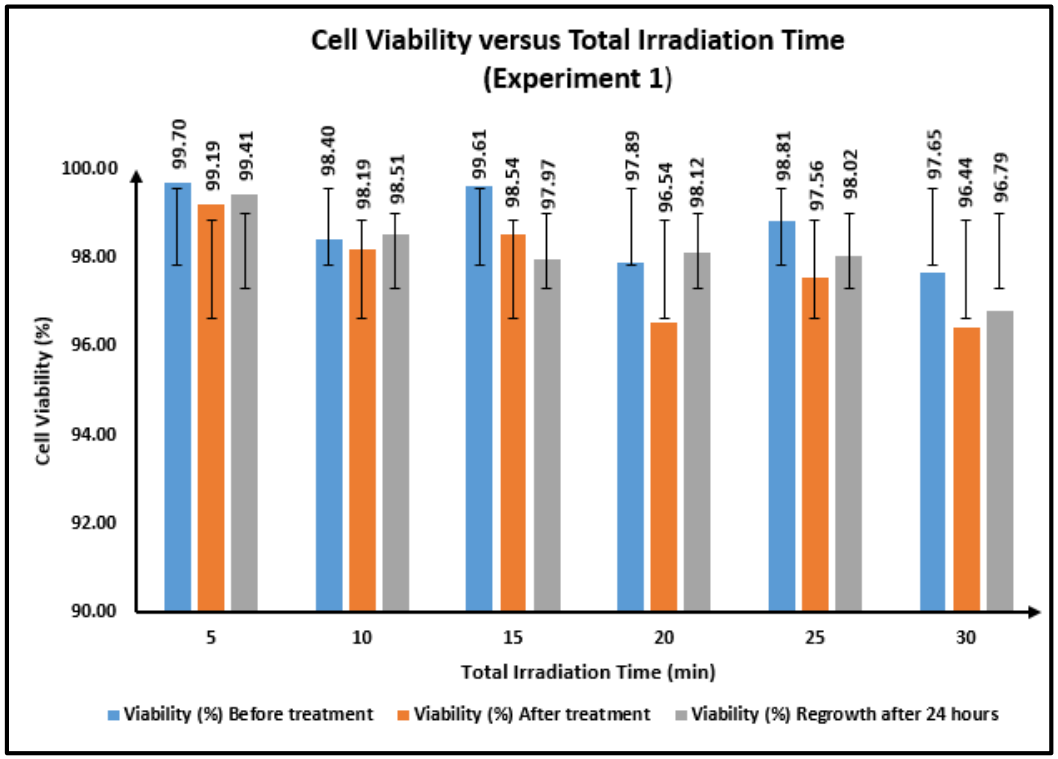

Enlarged Bar Chart of Figure 4.6(b).

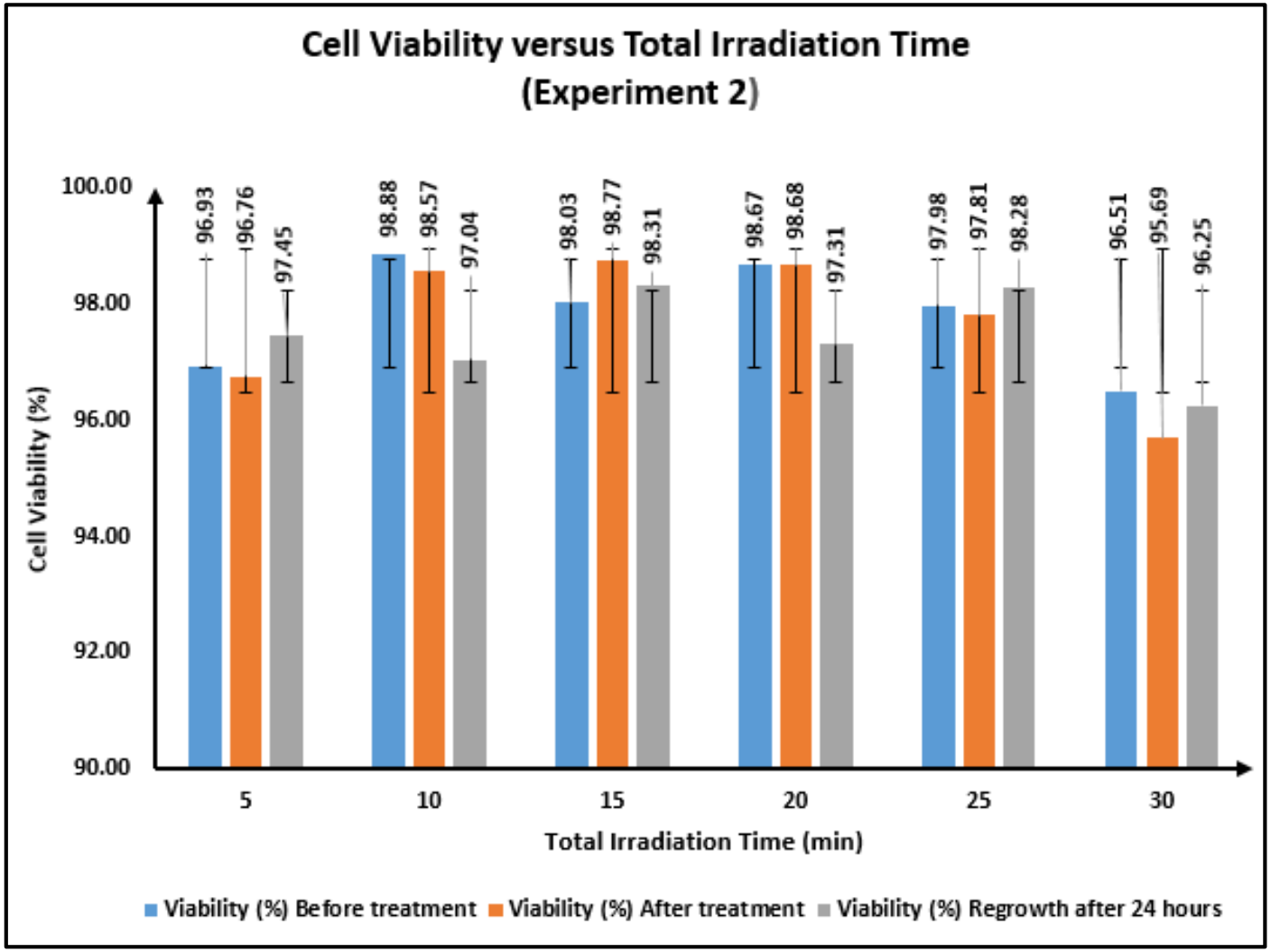

Enlarged Bar Chart of Figure 4.6(c).

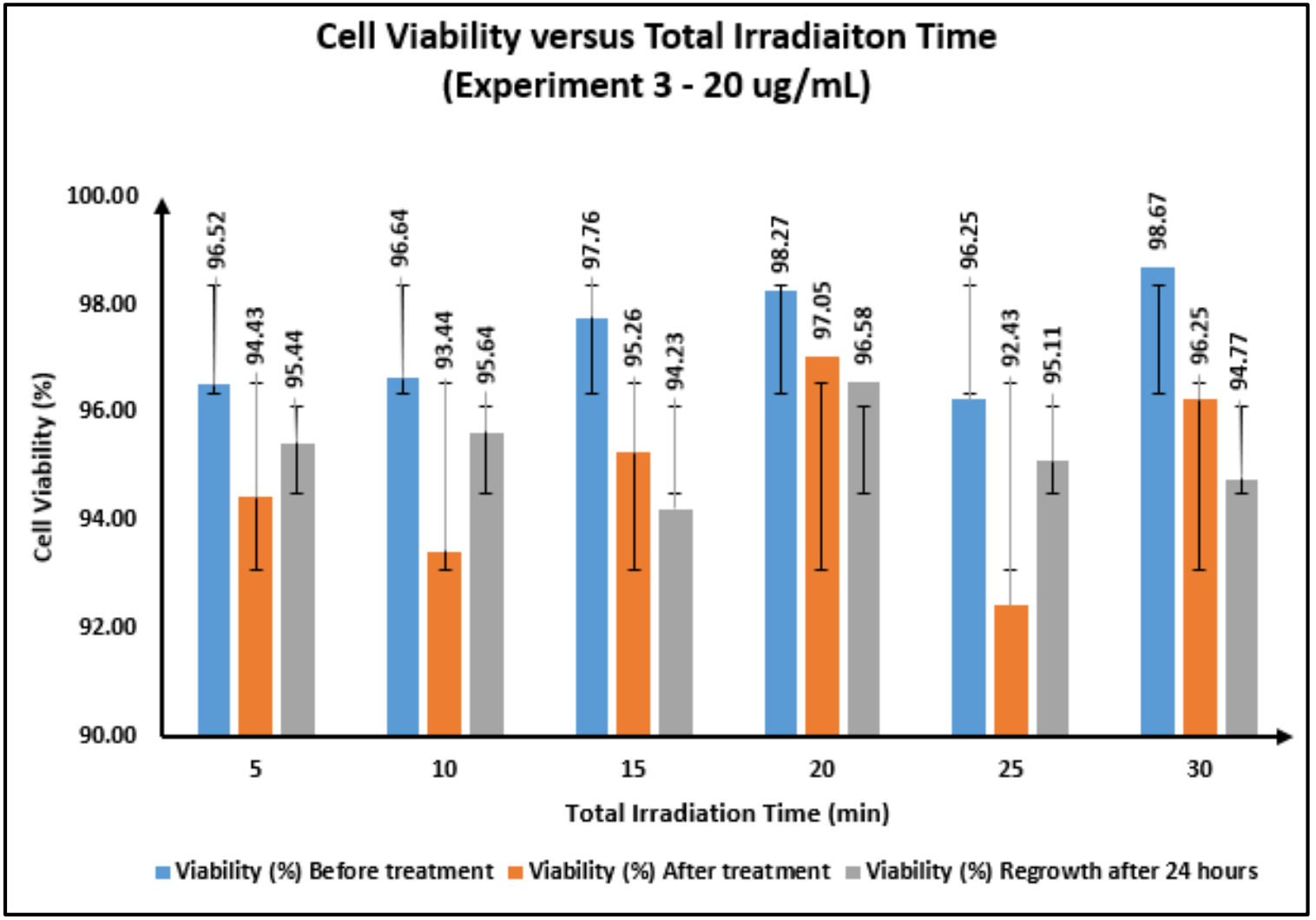

Enlarged Bar Chart of Figure 4.6(d).

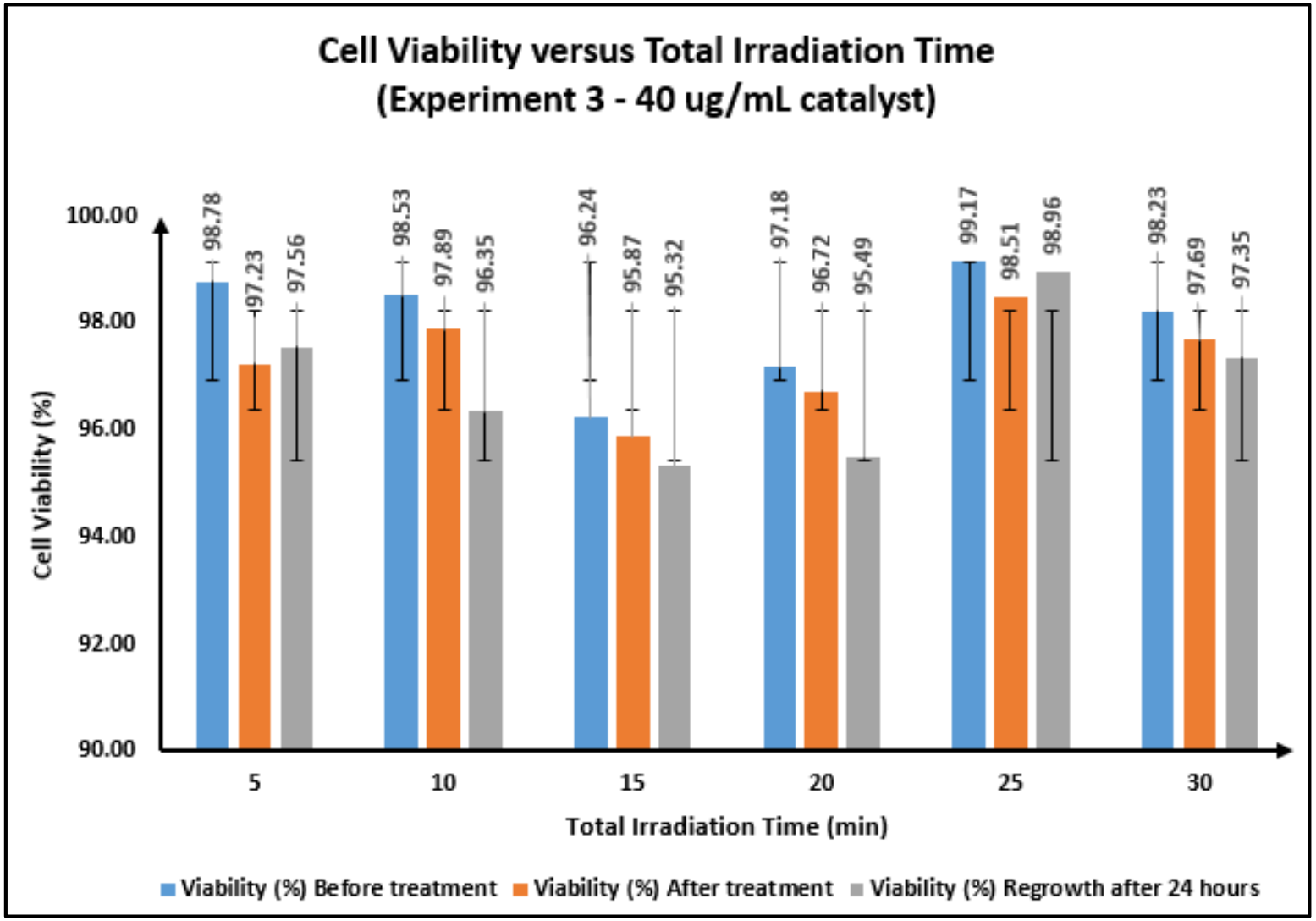

Enlarged Bar Chart of Figure 4.6(e).

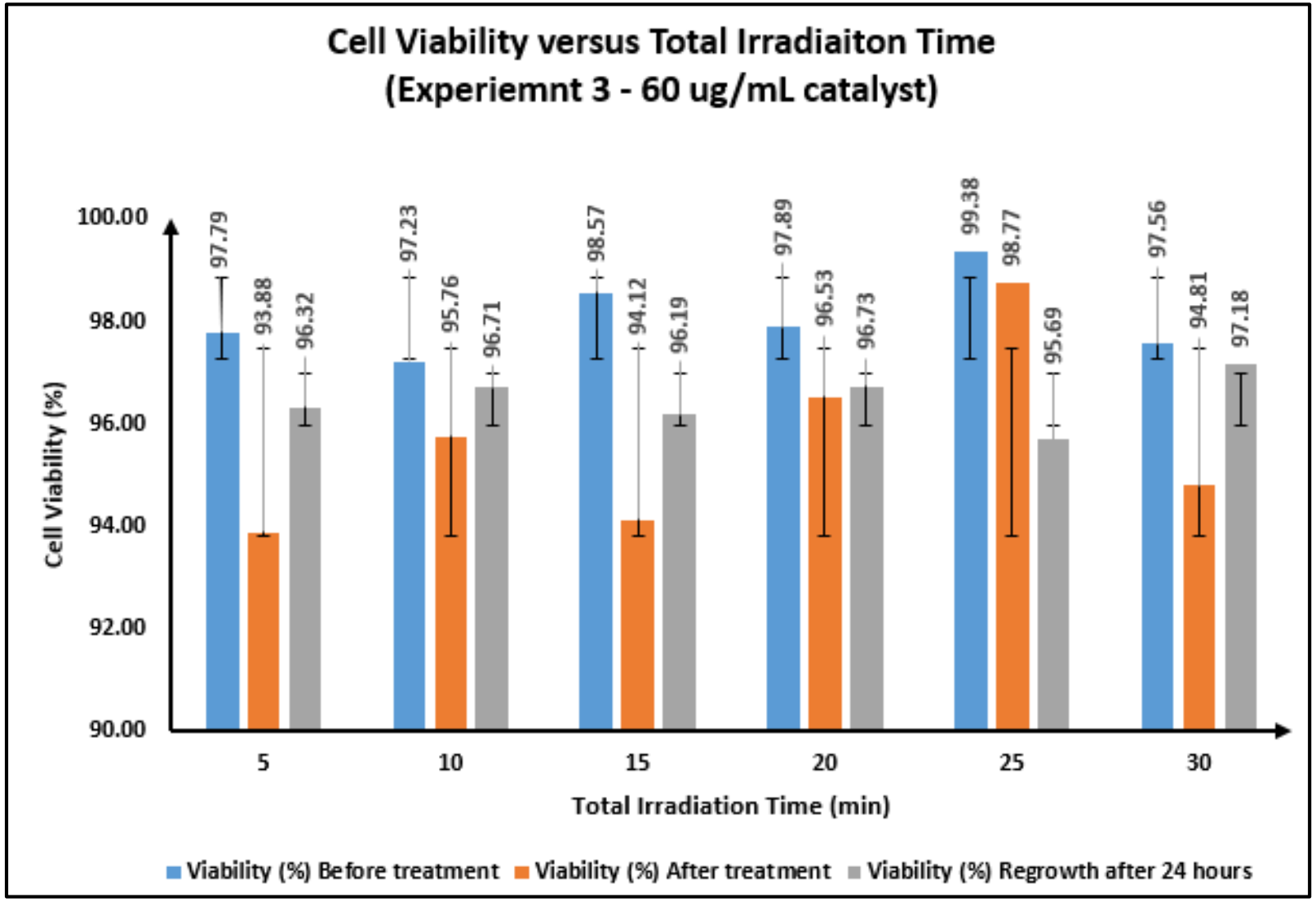

APPENDIX C: Enlarged Bar Chart of Figure 4.7

Enlarged Bar Chart of Figure 4.7(a)

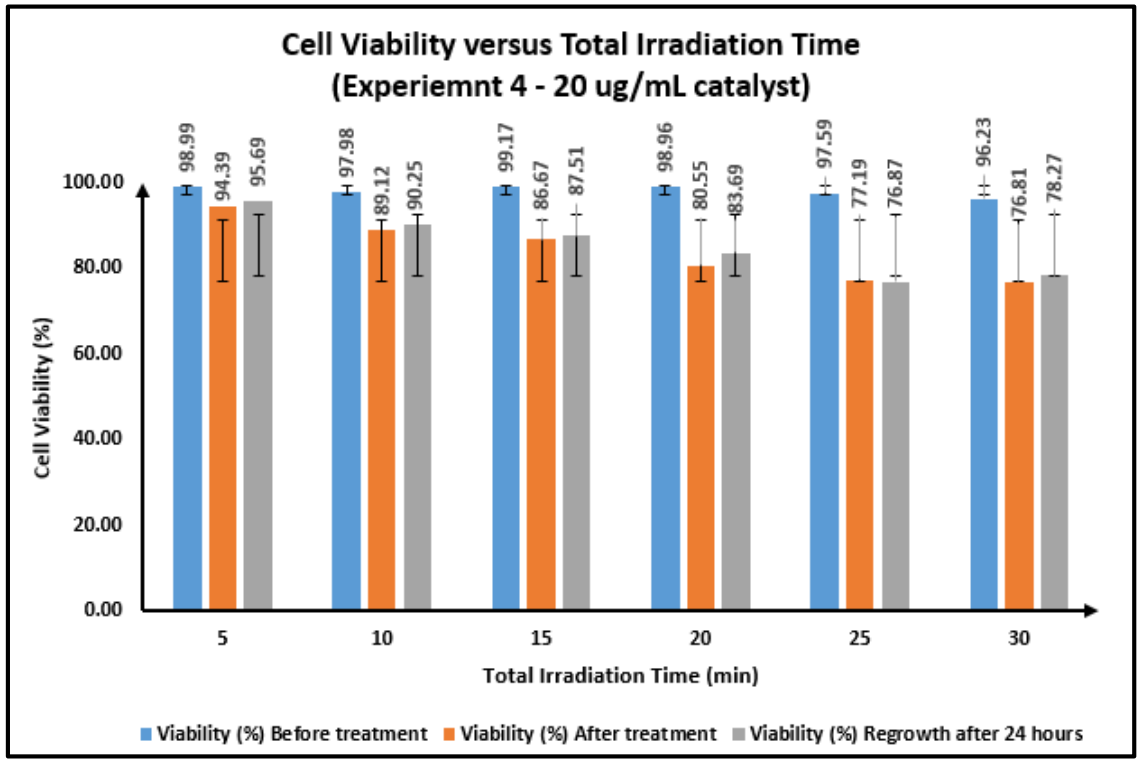

Enlarged Bar Chart of Figure 4.7(b)

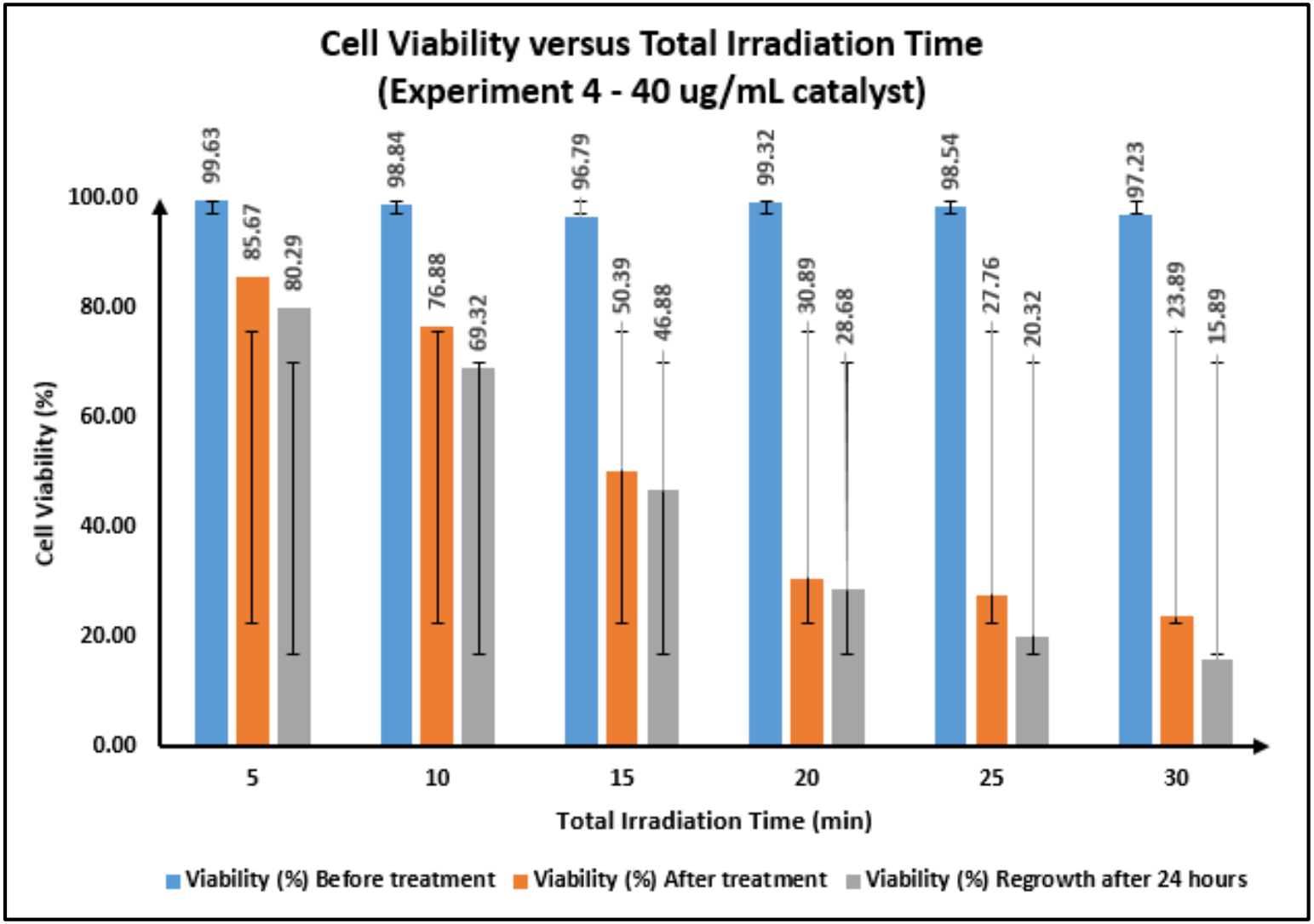

Enlarged Bar Chart of Figure 4.7(c)

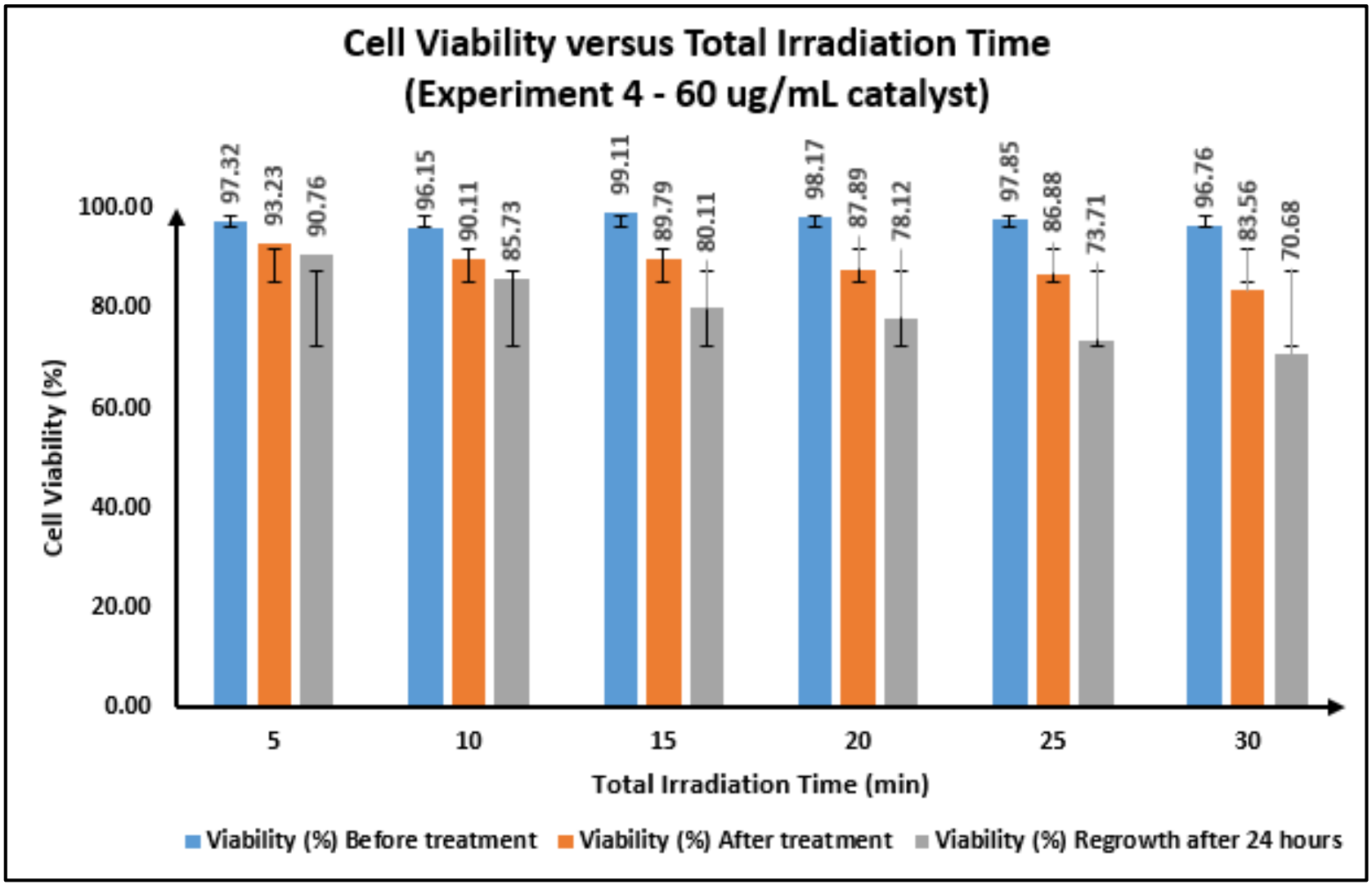

APPENDIX D: Enlarged Images of Figure 4.10

Enlarged Image of Figure 4.10 (a).

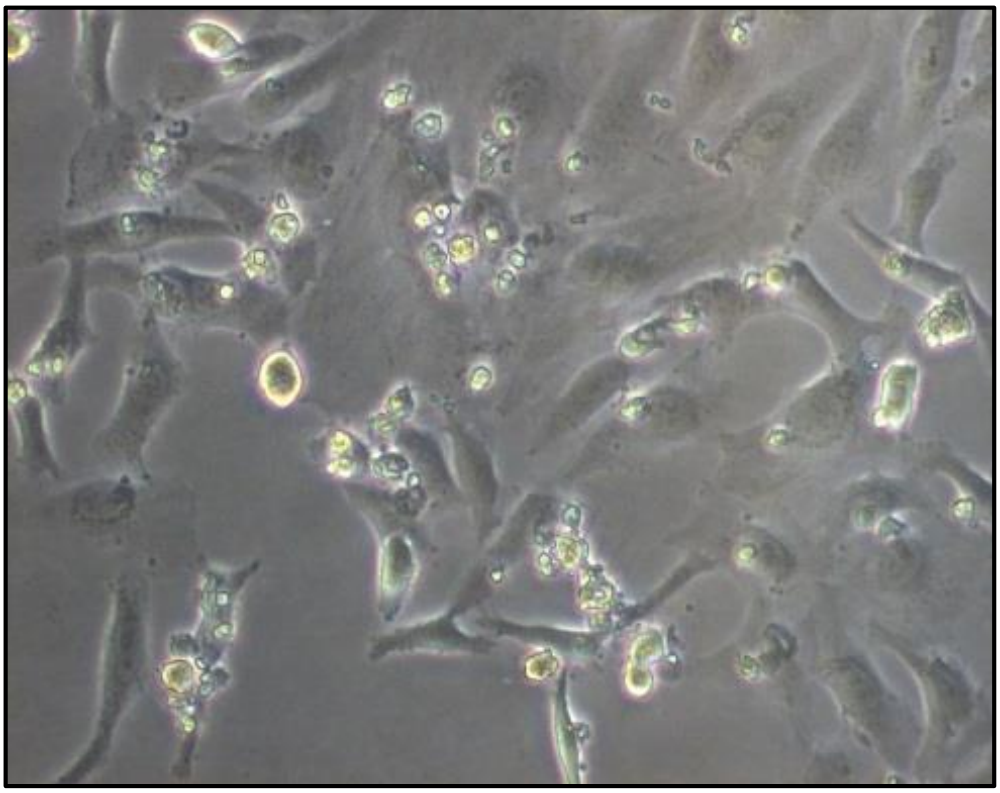

Enlarged Image of Figure 4.10 (b).

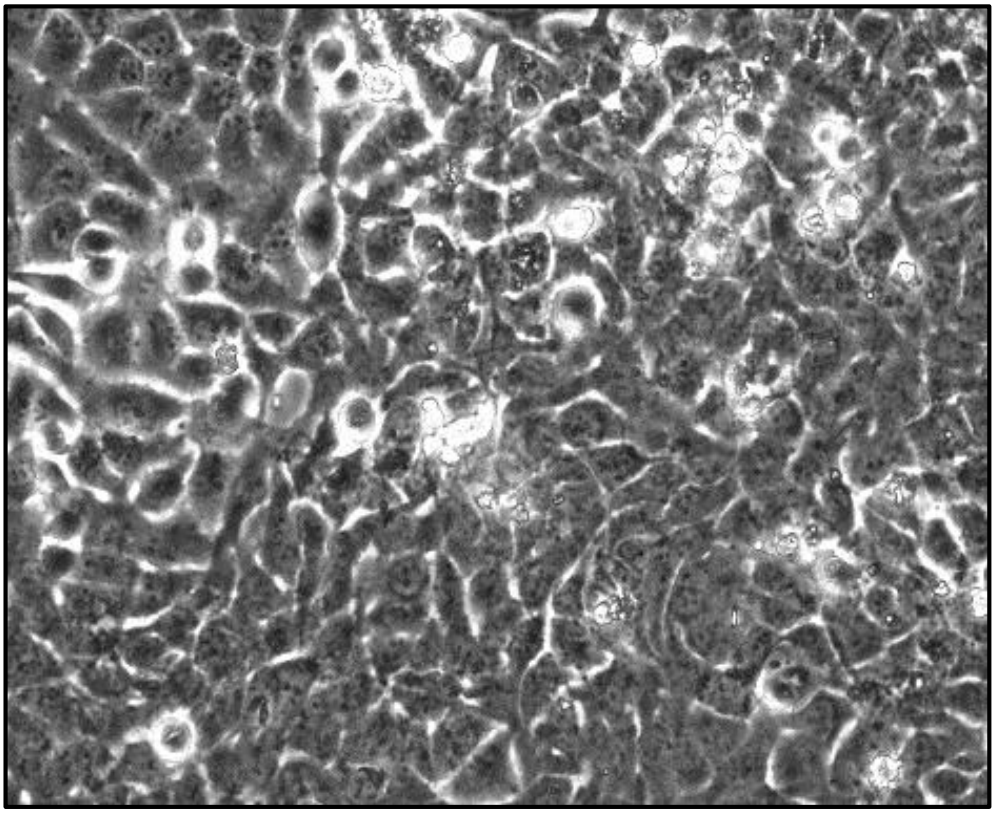

APPENDIX E: Enlarged Image of Figure 4.11

Enlarged Image of Figure 4.11 (a).

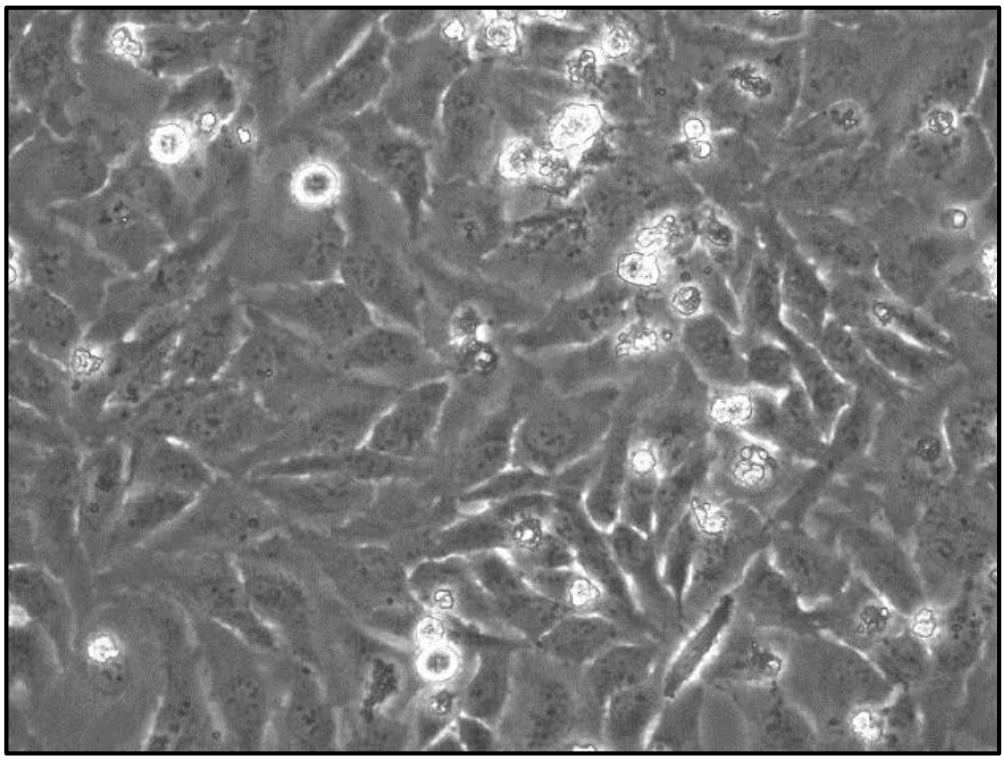

Enlarged Image of Figure 4.11 (b).

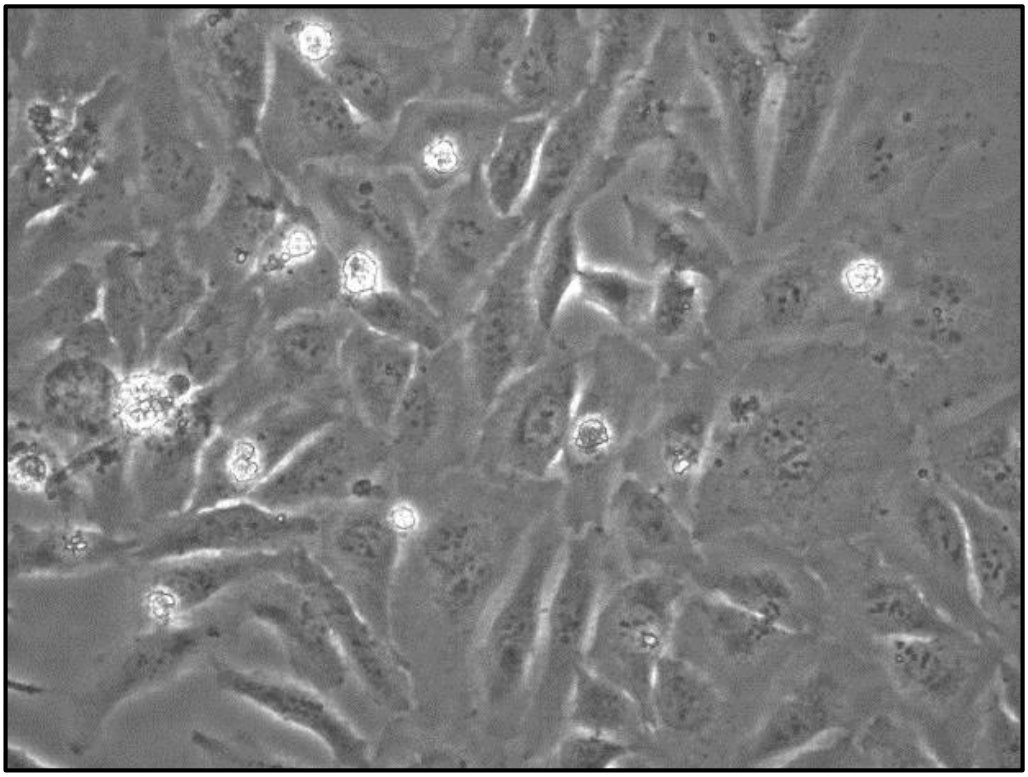

Enlarge Image of Figure 4.11 (c).

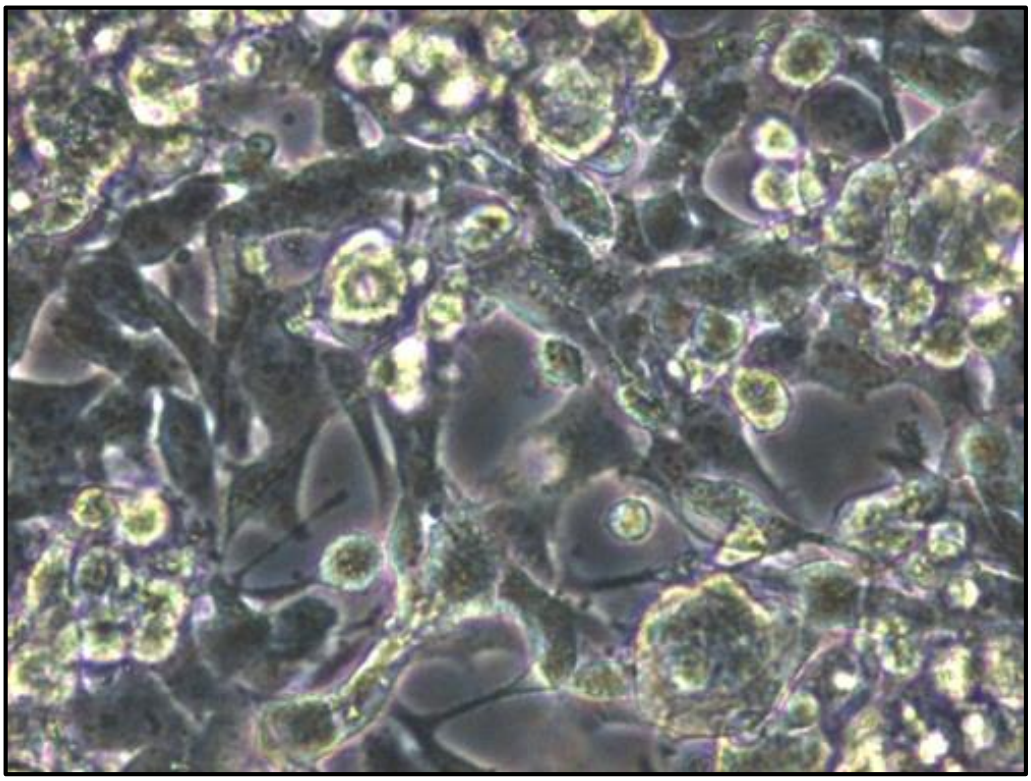

APPENDIX F: Enlarged Image of Figure 4.12

Enlarged Imaged of Figure 4.12 (a).

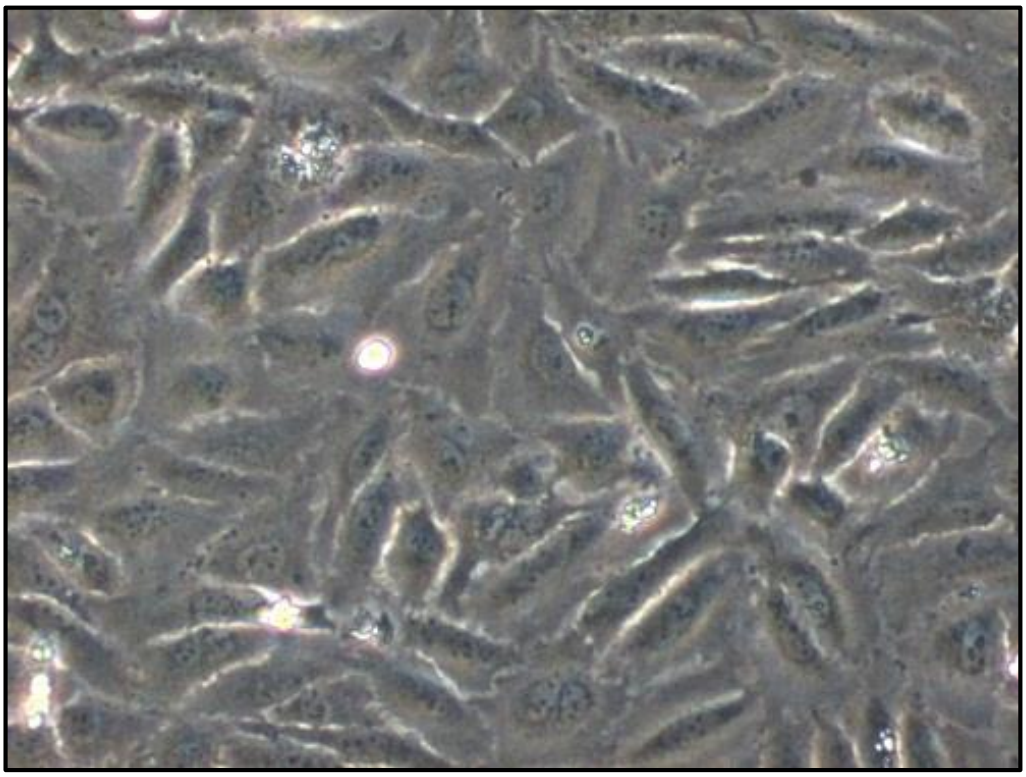

Enlarged Imaged of Figure 4.12 (b).

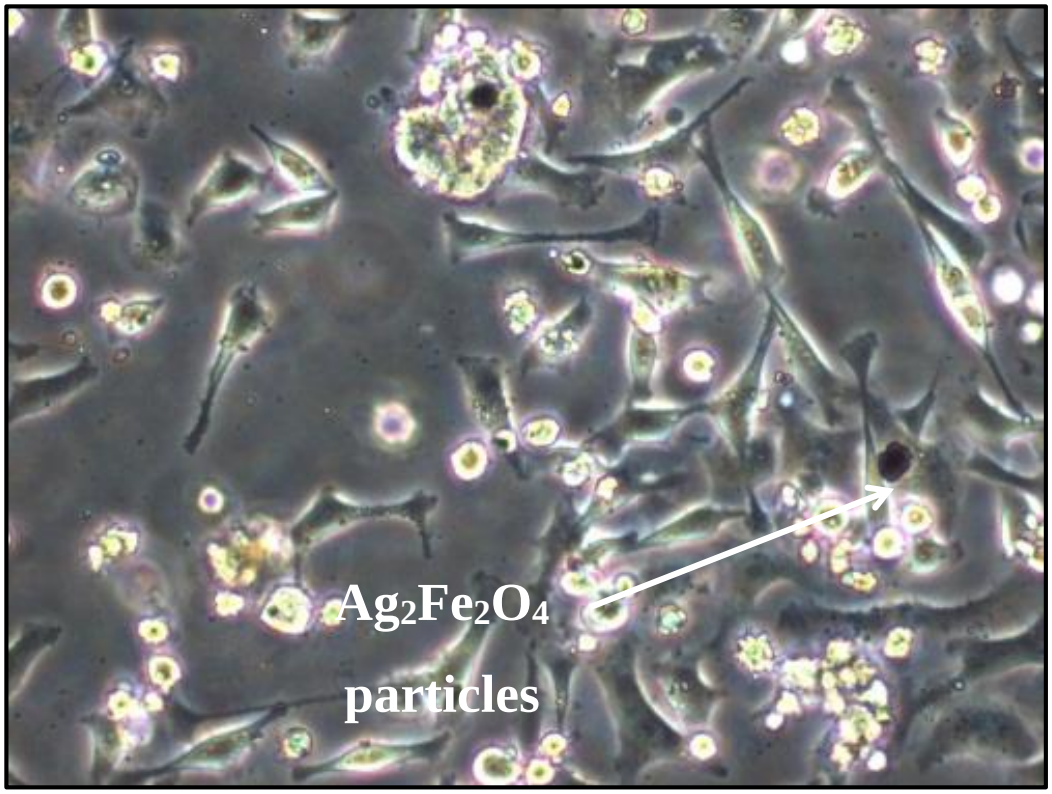

Enlarged Imaged of Figure 4.12 (b).

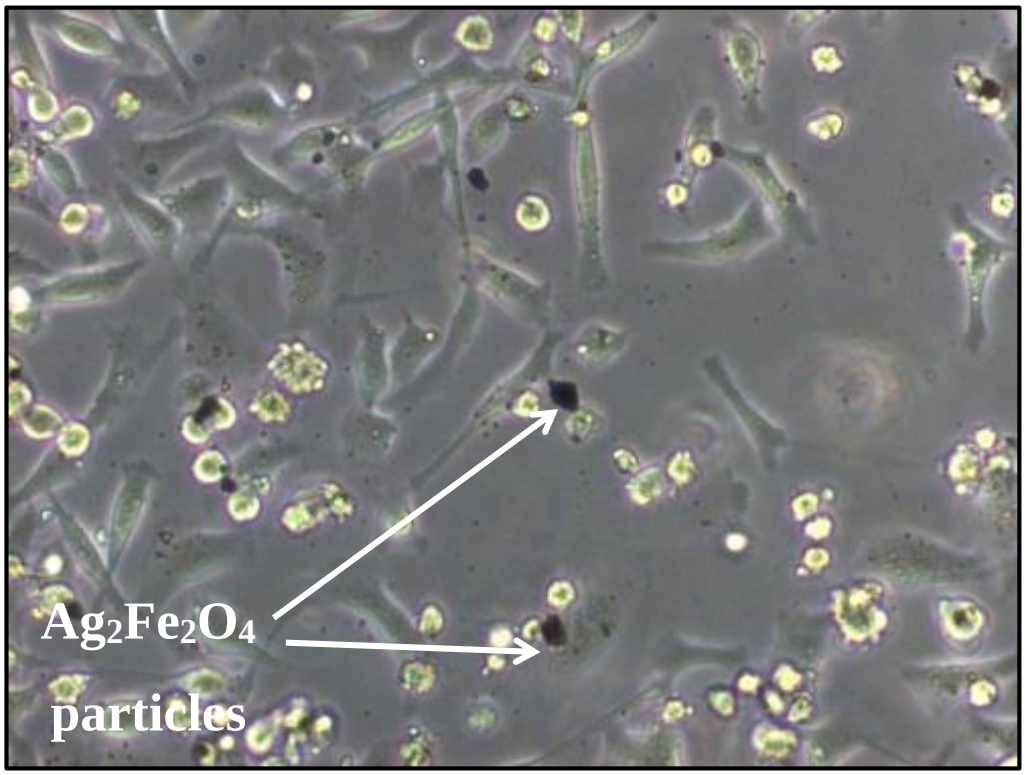

APPENDIX G: Enlarged Image of Figure 4.13

Enlarged Image of Figure 4.13 (a).

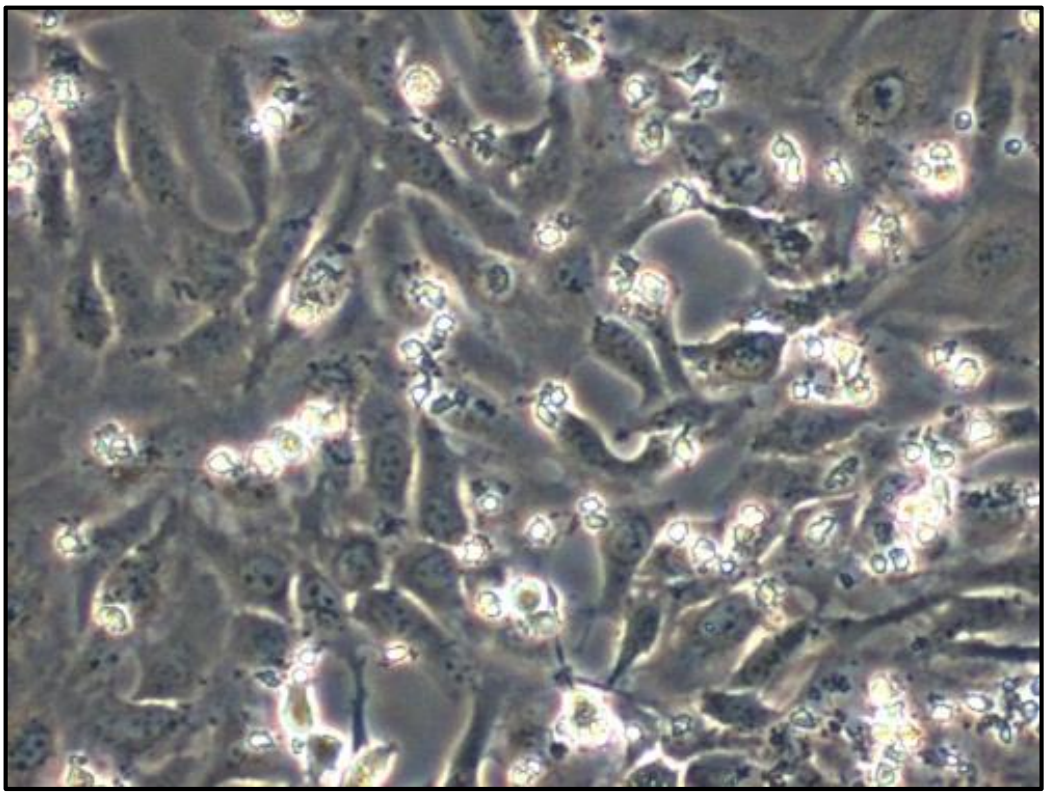

Enlarged Image of Figure 4.13 (b).

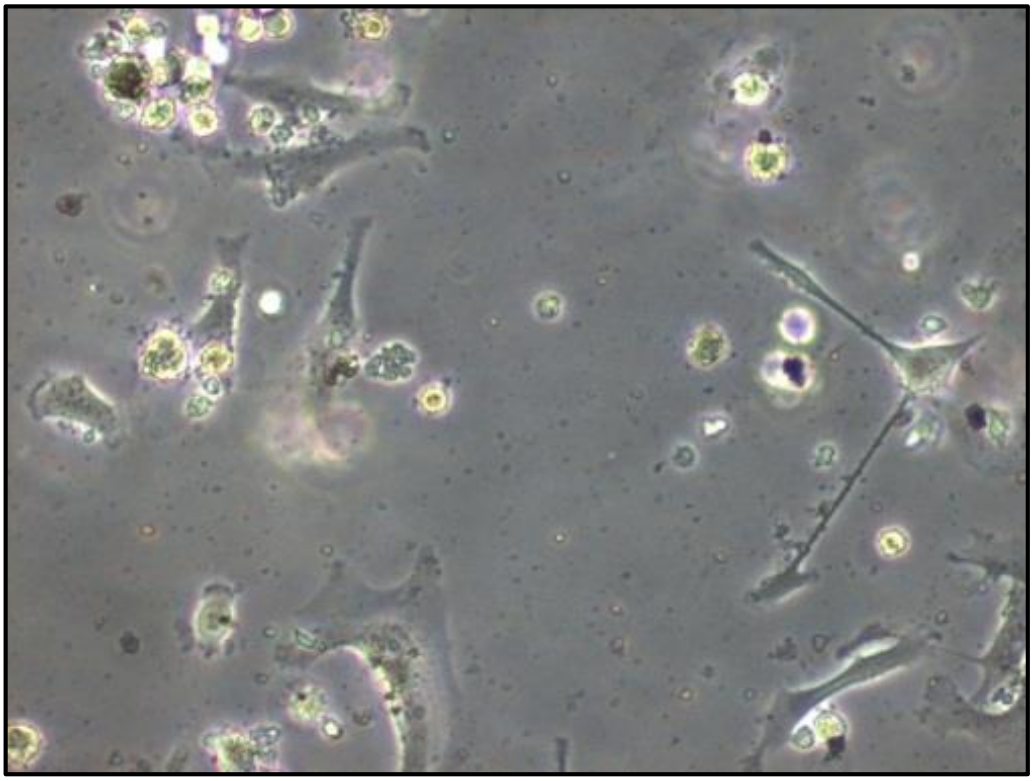

Enlarged Image of Figure 4.13 (c).

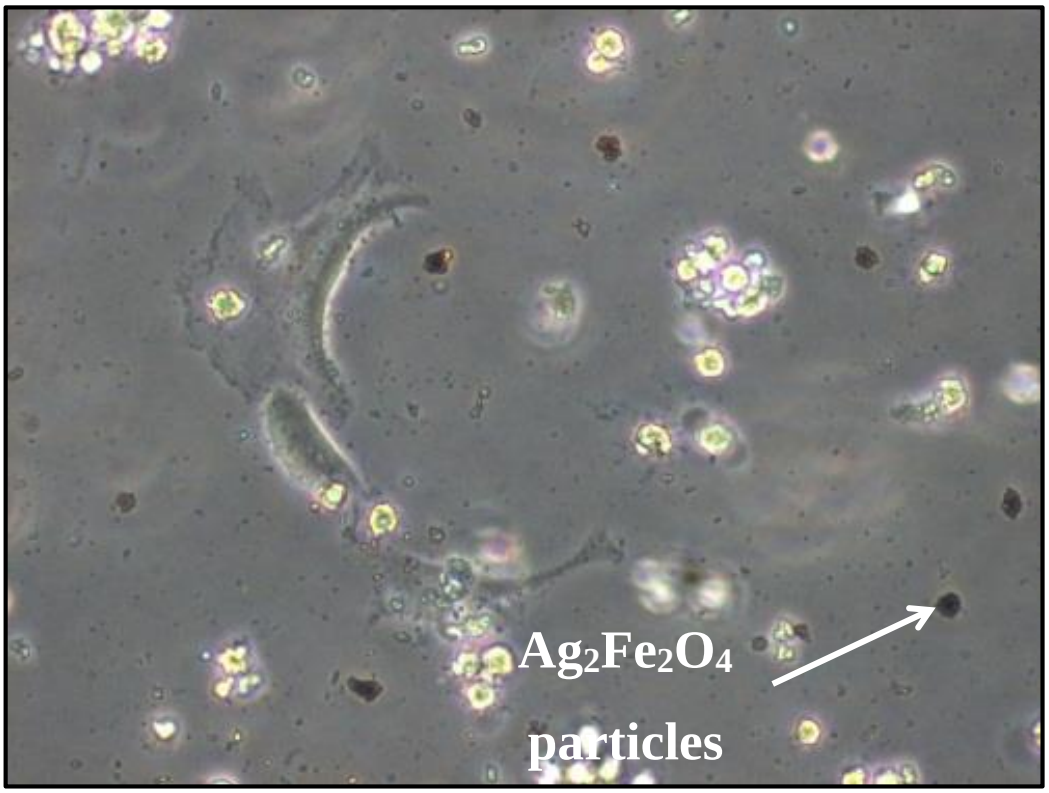

APPENDIX H: Enlarged Image of Figure 4.14

Enlarged Image of Figure 4.14 (a).

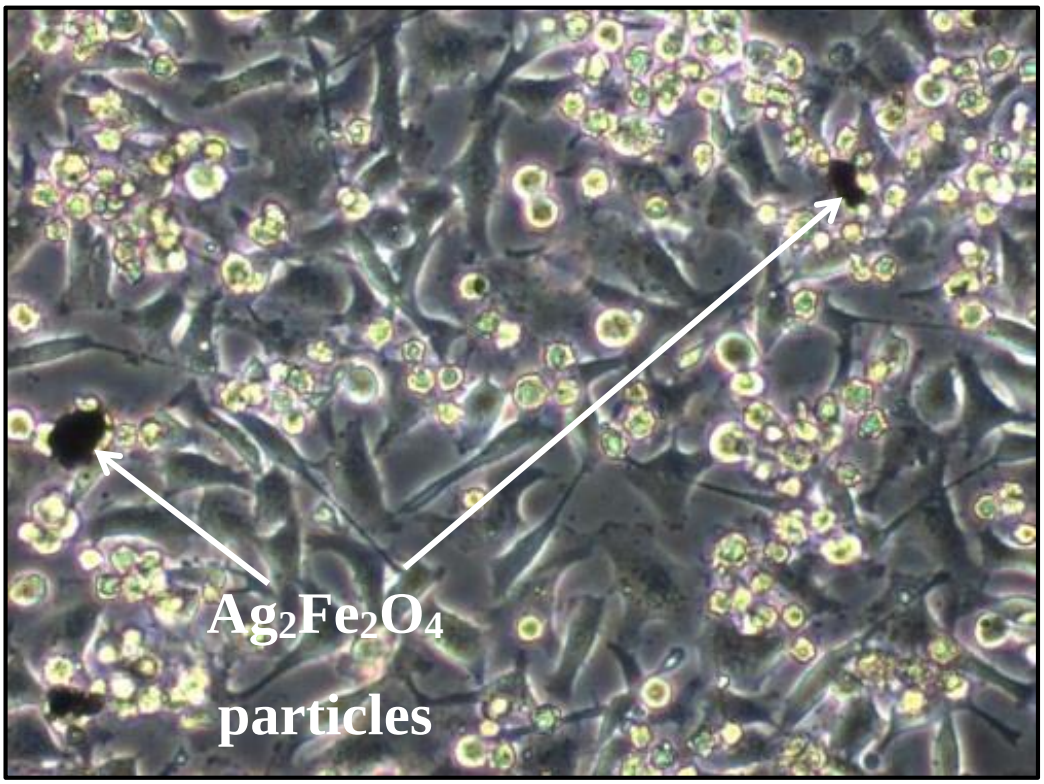

Enlarged Image of Figure 4.14 (b).

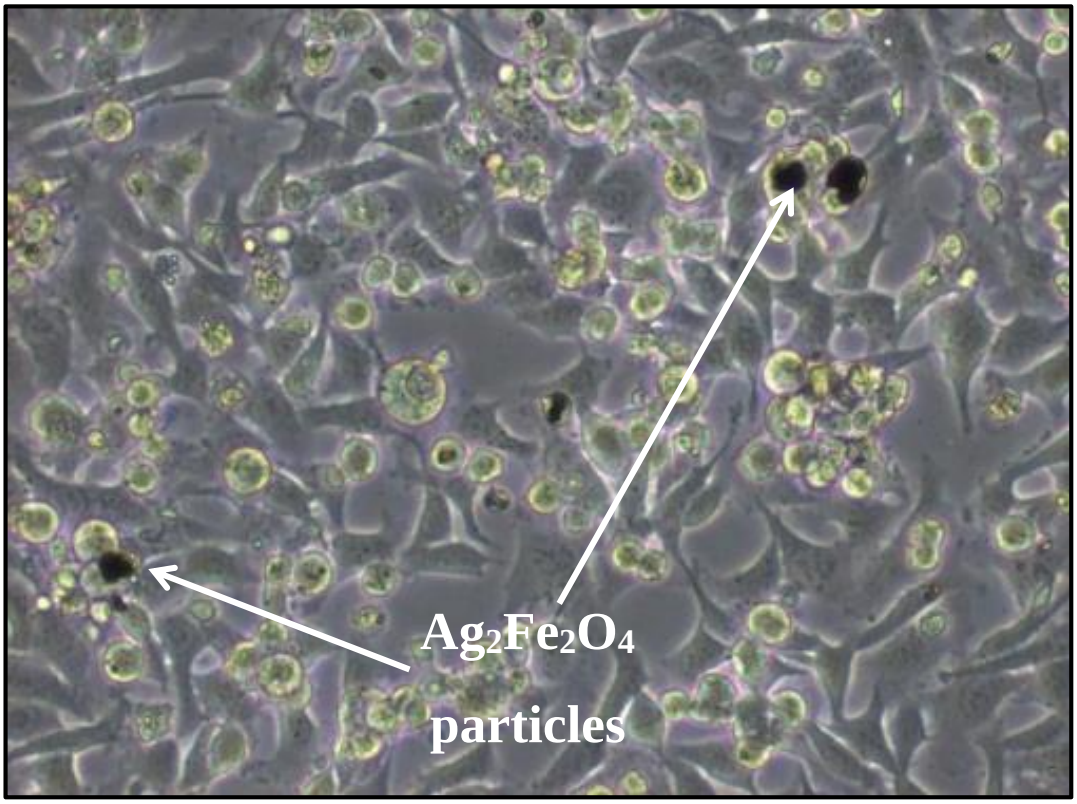

Enlarged Image of Figure 4.14 (c).